

Interannual variability in the tropical western Indian Ocean

M Manyilizu^{1,2*}, F Dufois³, P Penven⁴ and C Reason¹

¹ Department of Oceanography, University of Cape Town, Cape Town, South Africa

² College of Informatics and Virtual Education, University of Dodoma, Tanzania

³ Commonwealth Scientific and Industrial Research Organisation (CSIRO), Wembley, Australia

⁴ Institut de Recherche pour le Développement (IRD), Centre IRD de Bretagne, France

* Corresponding author, e-mail: majuto.manyilizu@gmail.com

A regional ocean model was used to study interannual variations in the Tanzanian shelf region and offshore in the tropical western Indian Ocean for the period 1980–2007. The model was forced with surface winds and heat fluxes from the National Centers for Environmental Prediction (NCEP) reanalysis, and its initial and lateral boundary conditions were derived from the Simple Ocean Data Assimilation (SODA). The weakest interannual sea surface temperature (SST) variations occurred in the coastal waters off Tanzania, where there was a strong correlation with waters to the north of Madagascar. The coastal waters were dominated by variability at a period of about 5 y. The strongest interannual SST variations occurred offshore, being dominated by two periods, one at about 2.7 y and the other at about 5 y. The variability of the region seemed to be linked to *El Niño*–Southern Oscillation (ENSO) and Indian Ocean Dipole (IOD) events that induced changes in the thermocline and surface heat fluxes in the region. Local surface heat flux exchanges driven by the anomalous shortwave radiation dominated the interannual SST variability in the Tanzanian shelf region, with some contribution by the advection of heat anomalies from the North-East Madagascar Current. Farther offshore, the interannual variability of the SST was dominated by the thermocline variations induced by local Ekman pumping from local wind stress curl and by remote forcing from large-scale climate modes.

Keywords: offshore, Tanzanian shelf

Introduction

The tropical Indian Ocean experiences strong, seasonally reversing winds. Generally, strong south-westerly and north-easterly winds blow in the austral winter (June–September) and summer (December–March) from and to the tropical western Indian Ocean respectively. Thus, austral winter and summer are correspondingly termed the South-West Monsoon and the North-East Monsoon. The transitions occur in April–May (spring) and October–November (autumn) with weak surface winds that are dominated by a westerly component along the equator (Schott et al. 2009).

The seasonally reversing winds in the tropical Indian Ocean influence the sea surface temperature (SST) and the upper ocean circulation. Weak winds in the transition periods correspond with significant SST warming, and these winds drive the eastward-flowing equatorial currents, termed ‘Wyrтки jets’. These jets are a combined response of direct forcing by semi-annual zonal equatorial winds (Wyrтки 1973), wave reflection (e.g. O’Brien and Hurlburt 1974) and basin resonance (Jensen 1993; Han et al. 1999). The strong winds during the South-West Monsoon lead to significant cooling in the tropical western Indian Ocean. The winds strengthen the East African Coastal Current (EACC; $\sim 2 \text{ m s}^{-1}$), which is supplied by the North-East Madagascar Current (NEMC) to the south, and the EACC supplies the northward-flowing

Somali Current (SC) to the north (Newell 1957; Figure 1a). During the North-East Monsoon, the north-easterly winds force the SC to flow southwards and also weaken the EACC ($\sim 0.2 \text{ m s}^{-1}$). This results in a confluence of the EACC and SC to form the eastward-flowing South Equatorial Counter-Current (SECC) (Newell 1957; Figure 1b). The reversing monsoon winds vary each year, resulting in considerable interannual variability (Webster et al. 1999). Such variability has been associated with the *El Niño*–Southern Oscillation (ENSO) (Reason et al. 2000; Annamalai and Murtugudde 2004; Schott et al. 2009) and the Indian Ocean Dipole (IOD) (Behera et al. 2000; Yamagata et al. 2004). Given that the tropical Indian Ocean forms the largest warm pool on Earth, which shapes both regional and global climate variability (Schott et al. 2009), any interannual change in its SST can lead to large-scale ocean–atmosphere variability. Thus, it is essential to gain a better understanding of SST variability in the tropical Indian Ocean.

The influences of the IOD and ENSO on the tropical Indian Ocean are phase-locked annually. An IOD event begins in late austral autumn/early winter, peaks during September–November, and most of the SST anomalies disappear by January of the following year (Vinayachandran et al. 2009). The SST anomalies in the tropical Indian Ocean basin develop slowly during an *El Niño* event, peaking in the

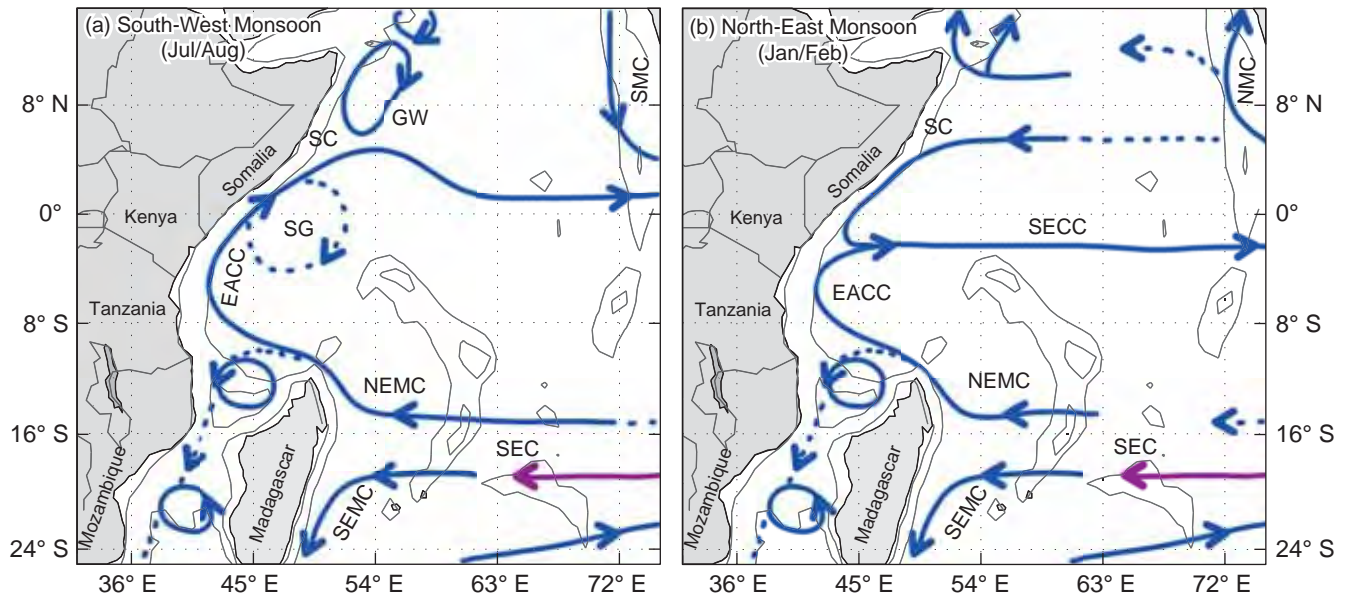


Figure 1: Schematic diagram of near-surface circulations in the tropical western Indian Ocean (in blue) and the subsurface return flow of the supergyre (in magenta) during (a) the South-West Monsoon and (b) the North-East Monsoon, adapted from Schott et al. (2009). Currents are the South Equatorial Current (SEC), South Equatorial Counter-Current (SECC), North-East and South-East Madagascar currents (NEMC and SEMC), East African Coastal Current (EACC), Somali Current (SC), Southern Gyre (SG), Great Whirl (GW), and South-West and North-East Monsoon currents (SMC and NMC)

austral autumn (March–May) following the *El Niño* onset year (Klein et al. 1999; Reason et al. 2000; Schott et al. 2009). ENSO-induced changes in the surface heat fluxes play a significant role in the northern Indian Ocean (Klein et al. 1999; Reason et al. 2000), as during an IOD event. However, the thermocline variability related to Rossby wave variations during ENSO or IOD events explains the strong SST variability in the south-western Indian Ocean, especially between 5° and 10° S (Xie et al. 2002; Schott et al. 2009). The anomalous Ekman pumping that forces the IOD-induced Rossby waves dominates to the north of 10° S, whereas ENSO-induced Rossby waves dominate to the south of 10° S (Rao et al. 2005; Yu et al. 2005).

The SST variability associated with the IOD or ENSO in the tropical western Indian Ocean greatly influences rainfall distribution. During positive IOD or *El Niño* events (e.g. 1997/1998), strong warming in the region may lead to intense rainfall, resulting in severe flooding in parts of East Africa (Ogallo 1988; Kijazi and Reason 2009; Schott et al. 2009). Additionally, the warm SST anomalies in 1997/1998 negatively affected coral reefs by increasing the level of coral mortality to about 50–60% (Obura et al. 2002). Devastating drought related to the strong SST cold anomalies occurs during negative IOD or *La Niña* events (e.g. 1999/2000; Schott et al. 2009). Farther south, SST anomalies in the south-western Indian Ocean have been reported to be associated with southern African rainfall variability (e.g. Mason 1995; Reason and Mulenga 1999). The variability of African rainfall affects the economies of eastern and southern African countries because drought leads to shortages of food and energy (hydroelectric power) and flooding causes disease outbreaks (e.g. malaria and cholera), as well as loss of life and property. Large

socio-economic effects related to rainfall patterns have been observed in East African countries, where livelihoods strongly rely on rain-fed agriculture, fisheries and hydroelectric power supply (Slingo et al. 2004).

There are several studies (e.g. Behera et al. 1999, 2000; Schott et al. 2009; Collins et al. 2012) on the tropical Indian Ocean in general, and a smaller number (e.g. Schott et al. 1990; Swallow et al. 1991) on the Somali Current and EACC in the tropical western Indian Ocean. However, the relationship between the Tanzanian shelf and the region offshore in terms of SST variability, and the possible mechanisms responsible for this variability, are not well understood. Hence there is a need to investigate the relative effects of regional ocean circulation (e.g. large-scale and coastal currents) and atmospheric forcing, which may contribute to the spatial inhomogeneity of the interannual SST variability in the western part of the region. Together with gaining further insight into regional climate variability, an improved understanding of SST variability in the region, particularly the relationships between coastal waters and the open ocean, will contribute to better planning and management of climate-sensitive activities in the East African region. The current study uses a modelling approach to investigate the possible mechanisms and relationships associated with SST variability on the Tanzanian shelf and the region offshore, over the period 1980–2007.

Using the Regional Ocean Modeling System (ROMS), our study addresses the following questions: Does the interannual variability in SST in the Tanzanian shelf region vary from that offshore? What drives this interannual variability? How sensitive is the SST variability to the local surface heat fluxes and lateral boundary conditions?

Datasets and methods

Model description

ROMS is a numerical code originally developed at Rutgers University and at the University of California, Los Angeles, USA, as an improvement of the S-Coordinates Rutgers University Model. The version used here is the Institut de Recherche pour le Développement (IRD), France, version of the code, ROMS AGRIF, available from <http://www.romsagrif.org> (Debreu et al. 2011). It is a free-surface, terrain-following ocean model that solves the three-dimensional, hydrostatic primitive equations (Shchepetkin and McWilliams 2003, 2005). It solves the equations using a split-explicit, time-stepping scheme and a free surface. Stretched, terrain-following coordinates are used in the vertical, and orthogonal curvilinear coordinates are applied in the horizontal on a staggered Arakawa C-grid. The surface heat flux is based on a bulk parameterisation at the air–sea interface (Fairall et al. 1996). Vertical mixing occurs through the K-Profile Parameterization (KPP) (Large et al. 1994).

Previous applications of ROMS in the western Indian Ocean have suggested that it can be used to model different physical processes in the Tanzanian shelf region at different time-scales. The ROMS model has been used extensively and successfully in a range of studies in the tropical western Indian Ocean (e.g. in the Zanzibar Channel [Mayorga-Adame 2007], in the South-West Indian Ocean [Penven et al. 2006], and in the tropical Indian Ocean [Hermes and Reason 2008, 2009]). It is, therefore, an established numerical tool for simulating ocean circulation in this region.

In our study, the ROMS model was configured in the tropical western Indian Ocean off East Africa for the domain 37.5°–60° E and 4.85° N–18° S. The configuration used a global topography dataset at 2' resolutions, processed by Smith and Sandwell (1997). The model aimed to assess the interannual variability in the tropical Indian Ocean for the period 1980–2007, with a 2 y spin-up time. It was forced with the National Centers for Environmental Prediction (NCEP) 6-hourly reanalysis using a bulk formula (a linear temporal interpolation was used throughout the course of the model simulation).

Although the NCEP winds that were used to force the model were coarser in spatial resolution than QuikSCAT (NASA's Quick Scatterometer), this difference was not expected to lead to significant errors because the western boundary current region of interest here (NEMC, EACC) responds more to remote forcing (e.g. wind stress curl over the whole basin) than is the case for eastern boundary currents. Differences between NCEP, ERA (ECMWF reanalysis) and QuikSCAT winds over the western Indian Ocean have been analysed by Collins et al. (2012). In their Figure 8, there are locally significant differences in seasonal mean wind stress curl between the two products near the coastlines and the various islands in the Indian Ocean, although the large-scale patterns are very similar.

The model initial and lateral boundary conditions were extracted from the Simple Ocean Data Assimilation (SODA) 2.0.2-4 (Carton and Giese 2008). The monthly values were used to force the lateral open boundaries by means of a linear temporal interpolation. The lateral boundary conditions

were based on a combination of active adaptive radiation conditions added to nudging (reaching a nudging time-scale of 360 days) and sponge (reaching a viscosity/diffusivity value of 1 000 m² s⁻¹) layers 150 km wide (Marchesio et al. 2001). The model simulation had 40 vertical levels, 1/6° horizontal resolution and time-steps of 1 800 s. The model outputs were averaged every two model days, which in turn were processed to calculate monthly and climatological data. The monthly anomalies of the interannual model output were extracted by subtracting the monthly climatological mean, calculated for 28 y (i.e. 1980–2007) of the model interpretation. This model run was termed the reference experiment (EXP_REF; Table 1).

The model was used to perform experiments to investigate the sensitivity of the ocean circulation – over the domain – to the local surface heat fluxes and lateral boundary conditions. These runs were conducted in order to understand the relative roles of the local surface heat fluxes and the lateral boundary conditions in the evolution of the interannual variability in the tropical western Indian Ocean. Two sensitivity experiments were conducted with the same domain configuration as the EXP_REF experiment. In those experiments, the interannual surface heat fluxes or lateral boundary conditions were replaced by a climatological equivalent in order to assess the relative importance of those two forcings on the interannual variability (Table 1). Those two runs were called EXP_CLIM_SODA and EXP_CLIM_FLUX respectively.

Datasets

The ROMS model used to investigate the variability in the Tanzanian shelf region was validated by comparing the model outputs with observations and satellite data. The SST data, extracted from the Advanced Very High Radiometer Resolution (AVHRR) Pathfinder (version 5) at 4 km horizontal resolution (<ftp://ftp.nodc.noaa.gov/pub/data.nodc/pathfinder>) and the Tropical Rainfall Measuring Mission (TRMM) Microwave Imager (TMI; ftp://ftp.ssmi.com/tmi/bmaps_v04/) at 0.25° horizontal resolution, were used for validation of the model SST for the same region. Further validation of the model was performed using Indian Ocean hydrographical data and the altimeter data. SST from the digitised global climatology on a 0.5° grid from the CSIRO Atlas of Regional Seas Version 2009 (CARS2009; www.marine.csiro.au) and the gridded Indian Ocean Hydrobase data (apdrc.soest.hawaii.edu) were used for further validation of the model in annual mean (data not shown). Moreover, our study benefitted from the direct *in situ* measurements of SST around Chumbe Island Coral Park (6°16' S, 39°10' E) in the Zanzibar Channel in the tropical western Indian Ocean (C Muhando, Institute of Marine Sciences, University of Dar es Salaam, pers. comm.). These data were recorded from 1997 to 2007 using data loggers that were tied to *Acropora* coral branches off Chumbe Island. There were sporadic missing data due to data logger detachment from the branches by either strong currents or fish bites. In addition, premature expiry of the temperature logger batteries sometimes caused data loss.

On account of the way the ROMS surface heat flux boundary condition is imposed, although no explicit restoring towards observed SST is used in the bulk formula,

Table 1: Descriptions of the ROMS experiments in the tropical western Indian Ocean

ROMS simulation name	ROMS configuration details		
	NCEP wind stress	NCEP surface heat flux	SODA lateral boundary conditions
EXP_REF	Interannual	Interannual	Interannual
EXP_CLIM_SODA	Interannual	Interannual	Climatology
EXP_CLIM_FLUX	Interannual	Climatology	Interannual

validating the model by comparison with the observed/satellite SST might not be a strong test of the model. In the model, atmospheric properties from the NCEP reanalysis are used to force a bulk formula (Fairall et al. 1996). In this context, the model SST is influenced by the NCEP atmospheric surface temperature, which is itself influenced by observed SST. In this regard, although not directly forced, model SST is not totally independent of observed SST. Thus, a stronger test involves comparing the ROMS sea surface height (SSH) with altimeter data, or the subsurface variables. Furthermore, validation of the ROMS model is provided by the altimeter SSH observations from Archiving, Validation and Interpretation of Satellite Oceanographic (AVISO). The altimeter SSH observations for AVISO were obtained for the period 1992–2007 at $\frac{1}{3}^\circ$ resolution (www.aviso.oceanobs.com). These are gridded data that combine altimeter measurements from different satellites using an interpolation mapping technique (Ducet et al. 2000). Our study used gridded maps of absolute dynamic topography. Owing to different absolute values of SSH in the ROMS simulation and the AVISO data that are due to their different reference levels, the spatial SSH deviations from their spatial mean are represented here.

The influences of ENSO and the IOD on the variability of the Tanzanian shelf region can be assessed through correlation analysis using the Niño3.4 index and the dipole mode index (DMI). ENSO and the IOD are prominent climate modes in the tropical Indian Ocean. The DMI is provided by the Japan Agency for Marine-Earth Science and Technology (JAMSTEC), which represents the difference of the monthly SST (the Hadley Centre Global Sea Ice and Sea Surface Temperature [HadISST] dataset for the period 1958–2010) between two boxes in the west ($50^\circ\text{--}70^\circ\text{E}$, $10^\circ\text{S--}10^\circ\text{N}$) and the east ($90^\circ\text{--}110^\circ\text{E}$, $10^\circ\text{S--}0^\circ$) of the tropical Indian Ocean (see www.jamstec.go.jp). The Niño3.4 index is extracted from the National Ocean and Atmosphere Agency (NOAA) and is the monthly SST anomaly averaged over $5^\circ\text{N--}5^\circ\text{S}$ and $120^\circ\text{--}170^\circ\text{W}$ (see gcmd.nasa.gov). It is commonly used to represent the SST variability associated with ENSO events.

Data analysis techniques

Analyses of the model results were performed using composites, correlation, empirical orthogonal function (EOF) decomposition, and wavelet analyses. All these techniques were applied to the monthly anomalies of the SST and forcing variables. The correlation and standard deviations (SD) of the monthly SST anomalies were computed from the ROMS model, AVHRR and TMI SST data.

The possible linkage between the interannual variations of the SST in the coastal ocean off Tanzania and the open ocean to the east was examined using correlation

analysis of this coastal region with the rest of the tropical western Indian Ocean. EOF analysis was used to identify the leading modes of the spatio-temporal variability of the SST in the region. The leading modes that explained more than 10% of the total variance of the SST variability from the EOF analysis were retained. The wavelet analysis was performed on the first leading principal components of the SST EOF and on the time-series of the selected locations in the domain using the Morlet wavelet (Torrence and Compo 1998). The analysis aimed to determine the time, intensity and duration of dominant modes produced by the SST EOF and the regions with important features. The wavelet analyses were performed on the time-series of the normalised box-averaged monthly SST in the coastal waters off Tanzania ($40^\circ\text{--}42^\circ\text{E}$, $8^\circ\text{--}10^\circ\text{S}$) and in the open ocean ($48^\circ\text{--}50^\circ\text{E}$, $0^\circ\text{--}2^\circ\text{S}$). The selected boxes were within regions of low and high SD of the monthly SST anomalies in the coastal waters and in the offshore region respectively.

Results

Annual cycle

The annual cycle of the ROMS realistic simulation (REF_EXP) was evaluated through the SST and SSH from observations and satellite data. These are key parameters commonly used for analysis of ocean–atmosphere interaction and dynamics of ocean circulation respectively. The SSH difference between high and low sea levels in the domain was higher than 40 cm in each month throughout the year, implying a dynamically active region. Given that the tropical western Indian Ocean experiences strong seasonality, it is useful to investigate its annual cycle, progressing from May, the monsoon transition season, to July, midway through the South-West Monsoon, followed by November, the next transition, and then to January, midway through the North-East Monsoon. Thus, the comparison between the model SST and the AVHRR SST, and the SSH with that from AVISO, was conducted for May, July, November and January (Figure 2).

In May, before the South-West Monsoon begins, the SST in the tropical western Indian Ocean warms above 28°C , and high SSH aligns with the dominant surface currents that form the basin-wide cyclonic tropical gyre. During May, warm SST values of between 28° and 30°C appear in a large area to the north of 10°S in the model and AVHRR data (Figure 2a, b). The warmest SST of about 30°C occurs in the north-east of the domain, and relatively cool SST (ranging between 27 and 28°C) appears to the east and north of Madagascar. This period is characterised by moderate winds, especially in the north-east (Figure 3a). Weak winds reduce the wind-induced evaporative heat loss and vertical mixing. In addition, the eastward-flowing Wyrтки

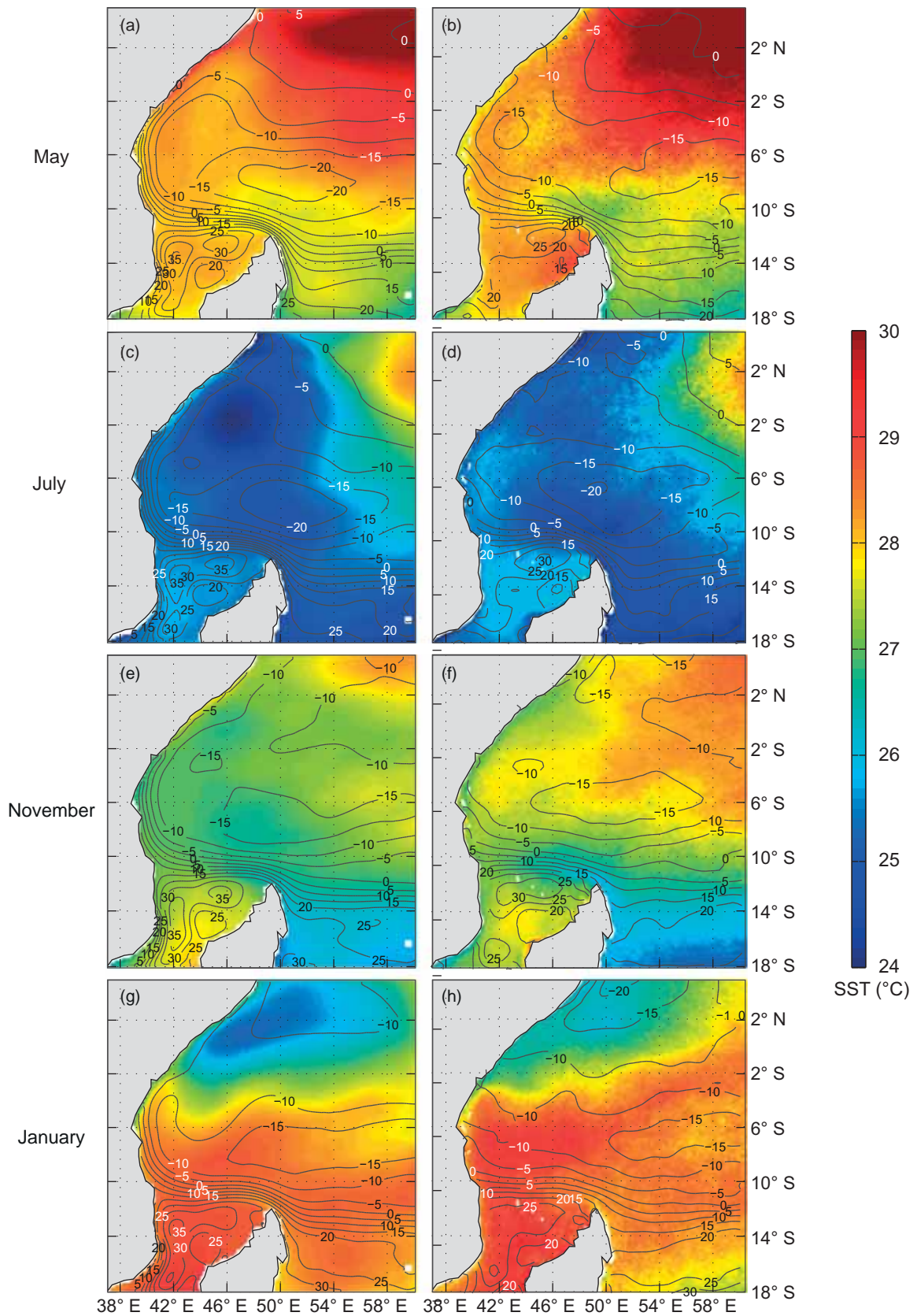


Figure 2: Annual cycle of sea surface temperature (SST; in colour) and sea surface height (SSH, cm; contours) over the tropical western Indian Ocean from the ROMS model (left column) and observation (AVHRR SST and AVISO SSH; right column) for (a, b) May, (c, d) July, (e, f) November and (g, h) January

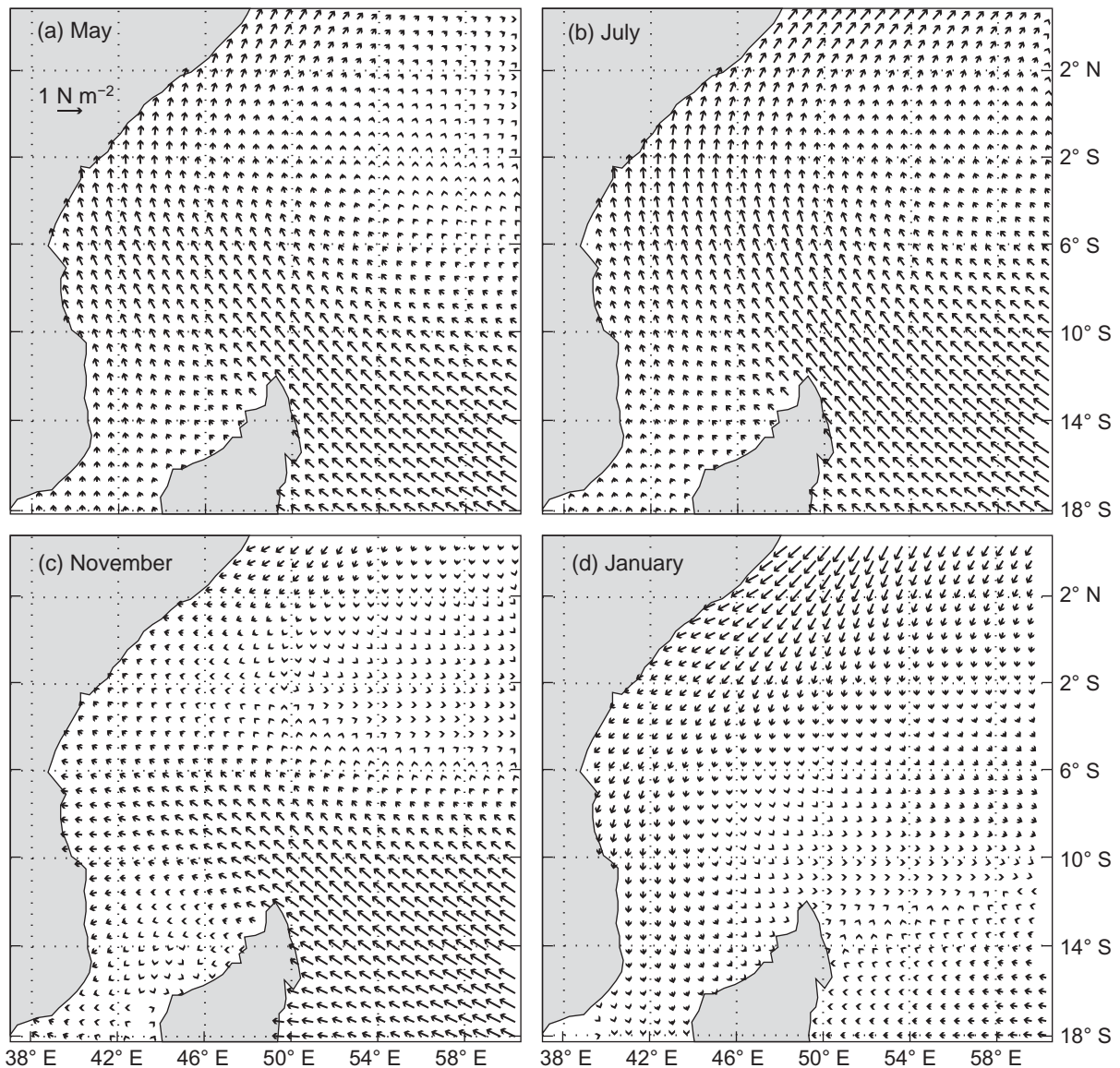


Figure 3: Annual cycle of wind stress over the tropical western Indian Ocean from the ROMS model for (a) May, (b) July, (c) November and (d) January

jets that develop during the transition periods carry warm waters from the west to the east. Thus, near the equator, the temperature of the tropical western Indian Ocean gradually increases towards the east in May. SSH contours in the model and AVISO align with the South Equatorial Current (SEC) and the NEMC to the south, the EACC to the west and the eastward-flowing Wyrtki jet to the north. The lowest SSH in the model simulation and the AVISO data occurs in the open ocean between 5° and 12° S. It is elongated and centred at 8° S, 52° E in the model simulation and farther east in the AVISO data.

The tropical western Indian Ocean cools significantly by July when the South-West Monsoon is fully developed (Figure 2c, d). Cool SST, ranging between 24 and 26 °C, appears over most of the tropical western Indian Ocean, except to the east of 54° E near the equator, in both the

model and AVHRR (Figure 2c, d). The coolest SST is attributed to the strong and steady monsoonal winds over the region (Figure 3b), which enhance both wind-induced evaporative cooling and vertical mixing. Furthermore, the cloudy skies that typically occur during this period reduce the solar insolation at the surface, and consequently reduce the net surface heat flux gain, leading to further cooling of the SST. High SSH patterns in EXP_REF and AVISO, that align with the SEC and the NEMC to the south, as well as with the EACC to the west, are maintained. The lowest SSH in the model simulation and AVISO between 5° and 12° S is contracted westward and centred at 8° S, 50° E.

During the transition period after the South-West Monsoon (November), the tropical western Indian Ocean warms (Figure 2e, f). The spatial patterns of SST from the model simulation and AVHRR range from 28 to 29 °C

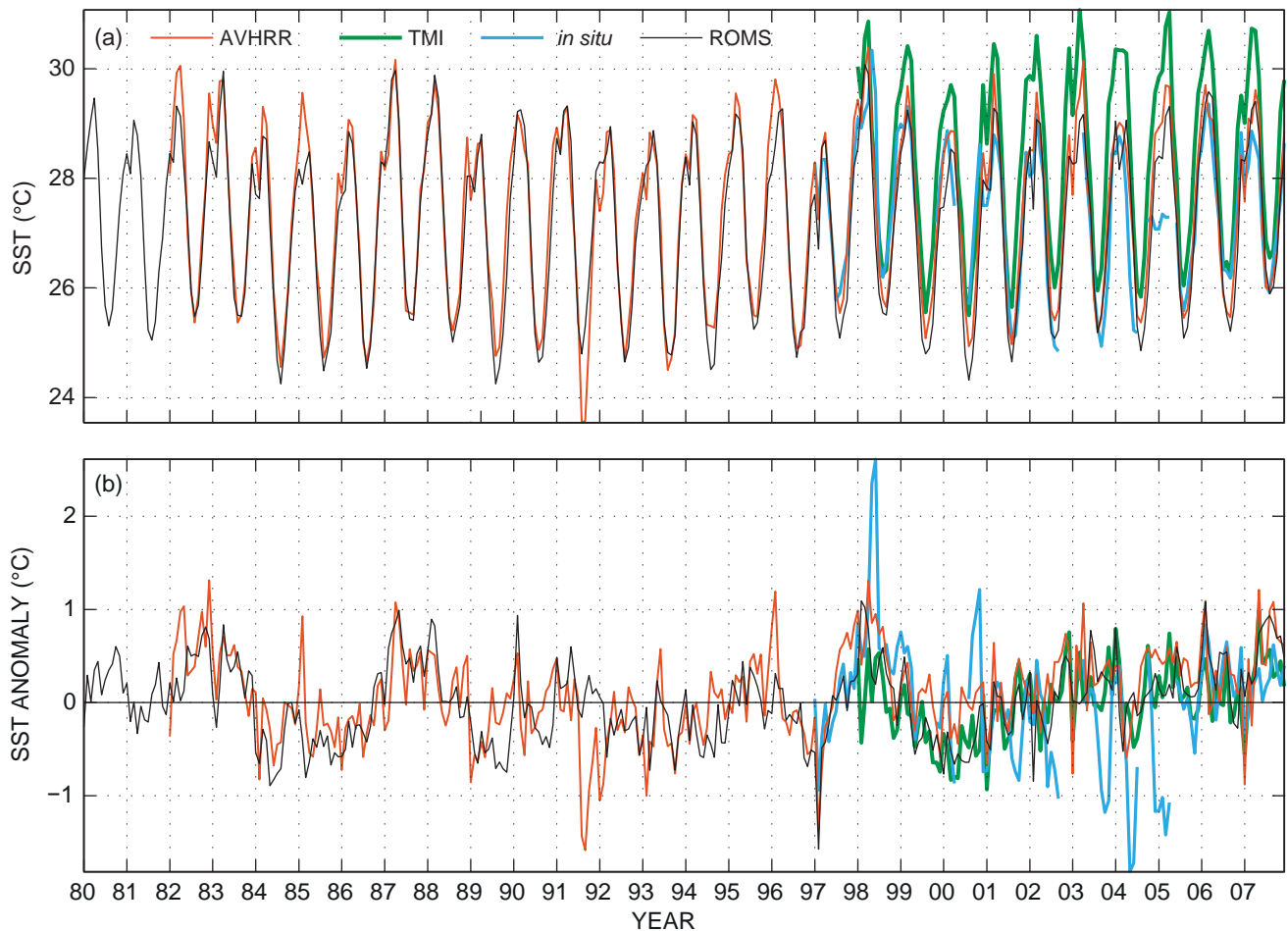


Figure 4: Time-series of (a) monthly SST and (b) monthly SST anomalies around the Chumbe Island Coral Park in the Zanzibar Channel from the ROMS model (1980–2007), AVHRR (1982–2007), TMI (1998–2007) and *in situ* data (1997–2007)

(Figure 2e, f). Relatively warm SST ($>27^{\circ}\text{C}$) to the north of 10°S can be associated with moderate winds (Figure 3c) that reduce the wind-induced evaporative heat loss and vertical mixing. In addition, the warming could be related to strong net surface flux due to the increased insolation as the sun moves across the equator from September. The Inter Tropical Convergence Zone (ITCZ) is near 2°S in October and moves southwards through November, resulting in strong shortwave radiation over the region. Two regions of low SSH patterns in the model and the AVISO data occur between 2° and 12°S .

During January, when the North-East Monsoon is underway, the SST shows a distinct north–south gradient in the model and the AVHRR data (Figure 2g, h). The zone of cooler waters of about $25\text{--}26^{\circ}\text{C}$ appears to the north of the equator and warms gradually towards the east and more rapidly to the south. A zone with warmer waters of about $28\text{--}29^{\circ}\text{C}$ appears to the south of the equator and it warms further in the northern Mozambique Channel. This SST gradient is associated with the circulation underlined by the -10 cm SSH contours shown for both ROMS and AVISO, and it separates the cooler zones of the north. Weak winds (Figure 3d), in conjunction with the position of the ITCZ near

12°S by the end of December, lead to warm SST in the southern tropical western Indian Ocean. SSH contours in the model and AVISO align with the SEC and the NEMC to the south, the EACC to the west and the eastward SECC to the north. The lowest SSH in the model and the AVISO data is elongated toward the open ocean between 5° and 10°S .

Generally, the ROMS model seems to reproduce fairly well the annual cycle in the tropical western Indian Ocean. The model SST and SSH agree reasonably well with the AVHRR and AVISO data respectively, which justifies their use in studying the interannual variability of the SST in the region.

Interannual variability of the SST

We used *in situ* measurements around Chumbe Island for the interannual validation in conjunction with the AVHRR and TMI SST data. The SST data corresponding to the region around Chumbe Island were extracted between 39.5° and 40.5°E and 6° and 7°S from the model, AVHRR and TMI. Thus, the time-series of the averaged monthly SST and SST anomalies from the model are compared against the AVHRR, TMI, and *in situ* SST data around Chumbe Island (Figure 4). The time coverage is 1980–2007 for the model

output, 1982–2007 for AVHRR, 1998–2007 for TMI, and 1997–2007 for *in situ* data. There are sometimes large differences between the temperatures collected at Chumbe Island and the other products, possibly caused by the coastal position of the station. However, most of the time-series of the ROMS SST agree with the AVHRR, TMI and *in situ* SST data off Chumbe Island for interannual time-scales. The difference between ROMS and the observations is comparable to the difference between the different SST products. This suggests that the ROMS model that is forced with the NCEP can realistically simulate the interannual

SST variability in the tropical western Indian Ocean for the period 1980–2007. Therefore, the ROMS model forced with the NCEP may be used to investigate interannual variability and perform meaningful sensitivity experiments on the variability in the Tanzanian shelf region. Spatial and temporal variations of the interannual SST in the Tanzanian shelf region and farther offshore are discussed below.

Spatial patterns and temporal variations

Figure 5 shows the SD and variance of the monthly SST anomalies in Tanzanian shelf waters and the open ocean

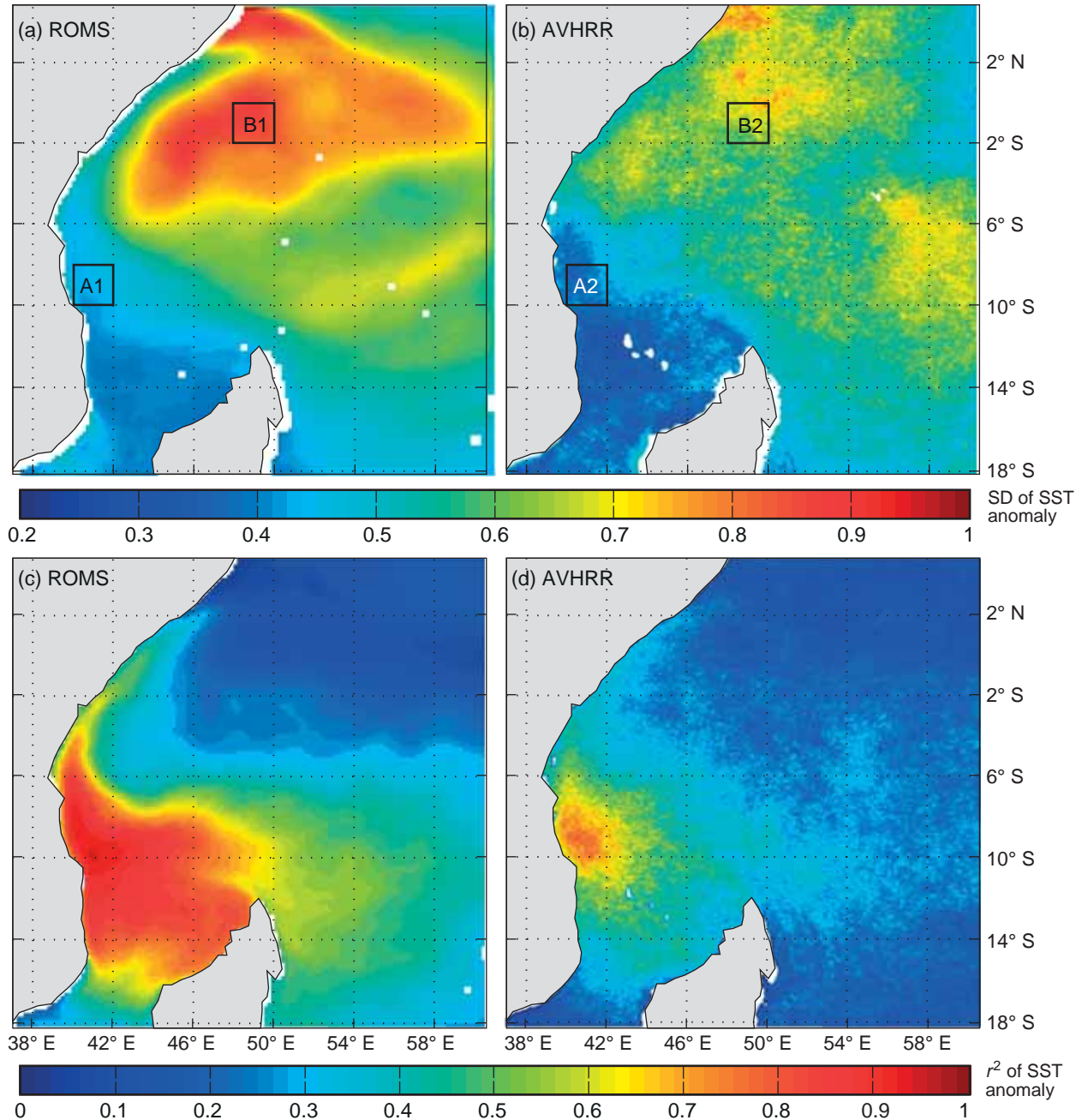


Figure 5: (a, b) Standard deviation of the monthly SST anomalies, with Boxes A1 and A2 representing coastal waters in the Tanzanian shelf region (40–45° E, 8–11° S) and B1 and B2 representing the open ocean (48–54° E, 1° N–2° S). (c, d) Square of the correlation coefficient between the monthly SST anomalies in the entire domain and those averaged over the coastal ocean, as extracted from Boxes A1 and A2

for the ROMS model and AVHRR data for a 25 y period (1982–2007). The smallest interannual SST variations are restricted along the coast up to 2° S and occur to the south of the domain in both ROMS (SD <0.4 °C) and AVHRR (SD ~0.5–0.6 °C). Thus, coastal variance is lower for ROMS and shows more spatial coherence than for AVHRR. Along with the differences in spatial and temporal resolution, this could be related to the local surface-forcing as well as to coastal instability processes that are not resolved by the model. The weakest variability in the Tanzanian shelf region links to the north and east of Madagascar, marking the NEMC and the northward-flowing EACC. The highest interannual variations of the SST in the region (SD >0.8 °C) are located offshore to the north of 6° S and are tilted to the north-east. Similar spatial patterns and magnitude in the interannual SST variations in the tropical western Indian Ocean also appear in the TMI dataset (data not shown). Such spatial patterns and magnitude in the monthly SST anomalies justify the analysis of the difference in interannual SST variability between the Tanzanian shelf waters and the open ocean. To investigate the origin of the interannual SST variability in the Tanzanian shelf region and in the open ocean, time-series (Figure 6) of the spatially-averaged monthly SST anomalies were extracted for the boxes depicted in Figure 5a, b respectively.

Figure 5c, d shows the correlation between SST in the Tanzanian shelf region and that over the rest of the tropical western Indian Ocean, expressed as its square (or the variance). Although the broad patterns are similar, there are several differences in the maps between ROMS and AVHRR. In general, there is more fine-scale structure in the AVHRR map, which may be a result of the 4 km horizontal resolution (see <ftp://ftp.nodc.noaa.gov>), which is substantially higher than the ~16 km or 1/6° horizontal resolution of the ROMS simulation. In both maps, the interannual SST variability in the Tanzanian shelf region appears to be linked with that to the north-west of Madagascar. However, there is no obvious link with that in the open ocean, especially to the north of 8° S. Hence we conducted further analyses of the interannual SST variability in the Tanzanian shelf region

and offshore using time-series and wavelet analysis (see below). These analyses assess the differences in time and frequency–time space of the SST variability between the Tanzanian shelf waters and the open ocean respectively.

Time-series and wavelet analysis

The time-series of the interannual SST variations in the Tanzanian shelf waters and the open ocean, from the model and AVHRR, are displayed together with the Niño3.4 index and the DMI (Figure 6). The analysis of the variability of these time-series was performed by filtering the monthly anomalies of the SST and the indices with a seven-month running mean to remove high-frequency variability. ROMS and AVHRR coastal time-series show a reasonably good correspondence for the long-term signals, whereas there are more differences for the higher frequencies. Such differences, e.g. in the SST amplitude depicted in Figure 5, could be related to local surface forcing as well as to coastal instability processes that are not resolved by the model. This could be tested using other surface forcing, but it is beyond the scope of our study which focuses on the interannual variability, whereas the differences seem to occur mostly at high frequencies.

Warm SST anomalies >0.5 °C in the model and AVHRR data occur for both the coastal and offshore region during 1982/1983, 1987/1988, and 1997/1998. These periods match the positive anomalies in the DMI and the Niño3.4 index (Figure 6), which is consistent with these being *El Niño* and positive IOD years. In addition to the abovementioned warm years, only the open ocean region indicates warm model SST anomalies >0.5 °C in 1980, 1991 and 2002/2003. The positive anomalies in 1980 and 2002/2003 correspond with negative and positive anomalies in the large-scale indices respectively. Thus, the warming in 1980 does not seem to relate to ENSO and the IOD because it is out of phase, whereas that in 2002/2003 does appear to relate to them because it is in phase. The model shows a large discrepancy in 1991, when the positive anomalies in the model SST, the DMI and the Niño3.4 index in both the

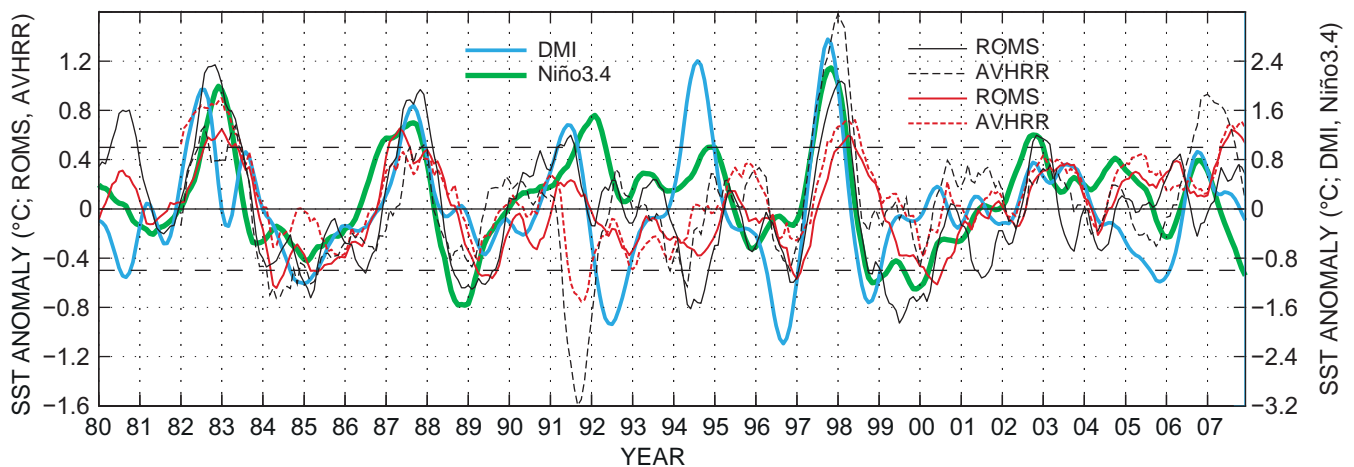


Figure 6: Time-series of the box-averaged monthly SST anomalies in the Tanzanian shelf region (in red; boxes A1, A2) and the open ocean (in black; boxes B1, B2) filtered with a seven-month running mean to remove any seasonal high-frequency variability. Boxes are defined in Figure 5. The DMI (in blue) and the Niño3.4 index (in green) are also shown

shelf waters and the open ocean occur at the same time as negative AVHRR SST anomalies. Moreover, in 1994 there is a greater positive anomaly in the DMI than in other indices. The years 1991 and 1994, respectively, were suggested to be pure positive IOD and *El Niño* by Tozuka et al. (2010). In summary, the Tanzanian shelf region and the open ocean in the tropical western Indian Ocean show commonality in the strong warm years ($>0.5^{\circ}\text{C}$) in 1982/1983, 1987/1988 and 1997/1998.

Strong, cool SST anomalies (less than -0.5°C) occur in 1984/1985, 1988/1989, 1996 and 1999/2000 in both the coastal and open ocean regions. Although these negative anomalies match the negative anomalies of the DMI and the Niño3.4 index, the 1996 event is most strongly evident in the DMI. The years 1992 and 1996 were suggested to be pure negative IOD events (Tozuka et al. 2010). However, the 1996 year seems to be a *La Niña* year as there are at least five conservative overlapping seasons with SST less than -0.5°C from August–October 1995 to

February–March 1996 (www.cpc.ncep.noaa.gov). The cold anomalies in 1984/1985, 1988/1989 and 1999/2000 are consistent with *La Niña* and negative IOD years. In addition to the cold years above, only the offshore region indicates cold model SST anomalies $>0.5^{\circ}\text{C}$ in 1994 and 2001. Negative anomalies of -0.4 – -0.5°C in 1994 appear also in the AVHRR data, and correspond with positive anomalies $>0.5^{\circ}\text{C}$ in the DMI and the Niño3.4 index. However, the negative anomalies in 2001 are not captured in AVHRR; instead, there are positive anomalies, with weak anomalies in the climate indices. In summary, the Tanzanian coastal waters and the offshore region show commonality in the strong cold years (less than -0.5°C) in 1984/1985, 1988/1989, 1996, and 1999/2000.

Wavelet analysis was performed on the time-series of the coastal and open ocean SST boxes for the model and AVHRR (Figure 7). AVHRR and ROMS show clear differences in their power spectrum which may be on account of differences in spatial and temporal resolution, as mentioned

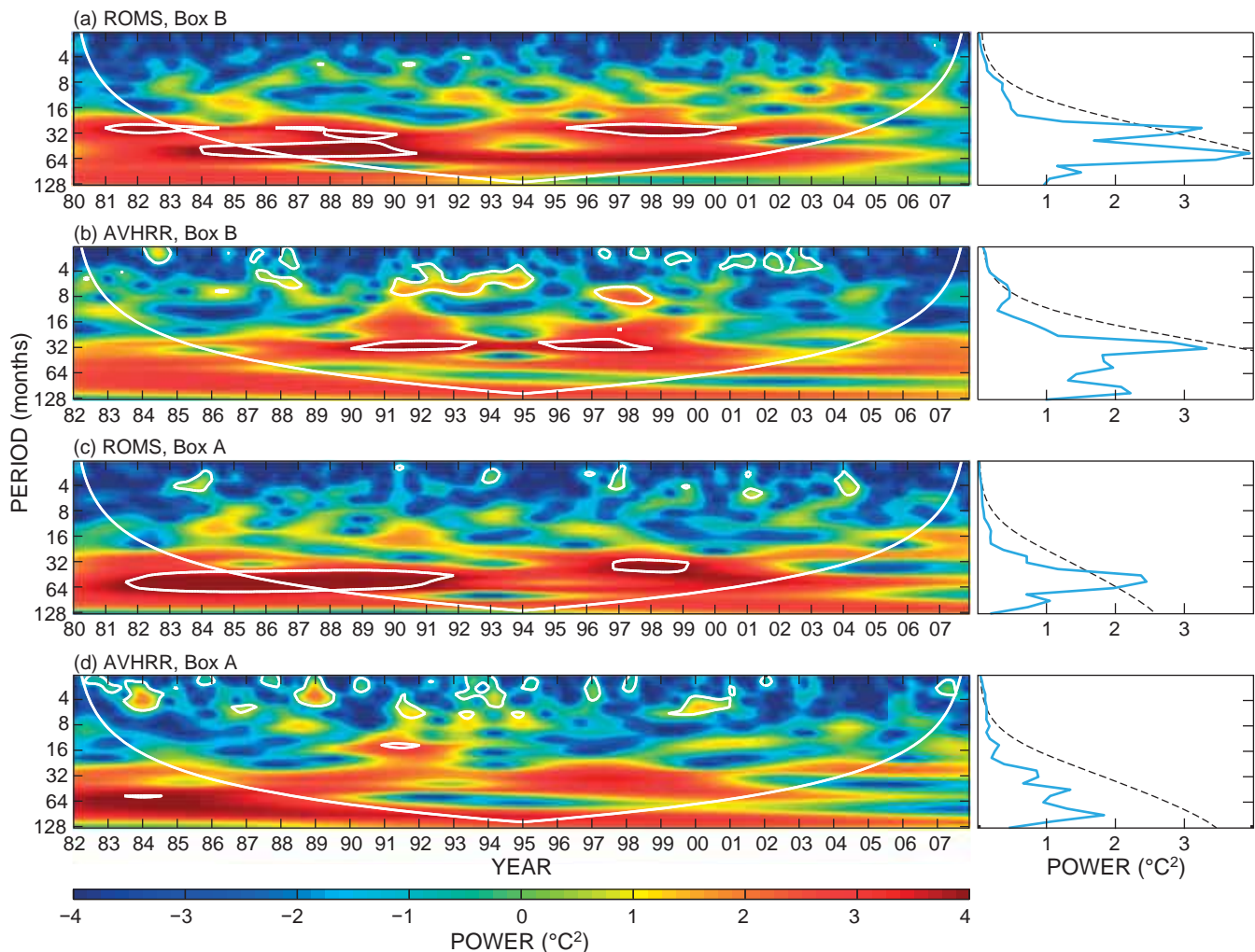


Figure 7: Wavelet power spectrum (left column) and power of the wavelet analysis (right column; blue line) of the box-averaged monthly SST anomalies in the open ocean (Box B) from (a) the model and (b) AVHRR, and in the coastal waters of the Tanzanian shelf region (Box A) from (c) the model and (d) AVHRR. Boxes are defined in Figure 5. The cone of influence is shown as a thin white line, as well as contours that indicate the 95% confidence level. Significance in the global wavelet spectrum is indicated by the black dashed line

above. Signals for a period of ~64 months appear in the coastal waters from 1982 to 1992 and 1997 to 1999 in the model SST. Similar signals also occur in the open ocean from 1984 to 1990 in the model SST. In the open ocean, a 32-month signal is also significant, whereas, in the coastal waters, signals for only the ~64-month period are significant. The difference in interannual variations between the Tanzanian shelf region and open ocean suggests either different forcing mechanisms or else the same forcing mechanisms over the regions, but where the SST in the two regions is modified differently by ocean processes and dynamics.

Surface heat fluxes and thermocline

In the Tanzanian shelf region, interannual variations of the mixed-layer temperature tendency correlate with only the local surface heat fluxes, which are driven by anomalous shortwave radiation (Figure 8a, b). In the shelf region,

anomalies of shortwave radiation and latent heat fluxes are out of phase (Figure 8b). This implies that enhanced latent heat loss (negative latent heat anomalies) occurs at the same time as positive anomalies of shortwave radiation (as in 1987/1988, 1997/1998, 2003 and 2005), whereas the reduced latent heat loss (positive latent heat anomalies) relates to the negative anomalies of shortwave radiation (as in 1984/1985, 1988/1989 and 1994–1996). The positive anomalies of the shortwave radiation over the Tanzanian shelf region can be associated with strong winds over the shelf and to the north of Madagascar, which carry away moisture and clouds during warm years, resulting in mainly clear-sky conditions. The opposite is the case during cold years in the Tanzanian shelf region. Figure 9a shows anomalies of the mixed-layer temperature tendency that are negatively related to anomalies of the mixed-layer depths and wind stress, with a small contribution of the wind stress curl (Figure 10). The local SST anomalies are then

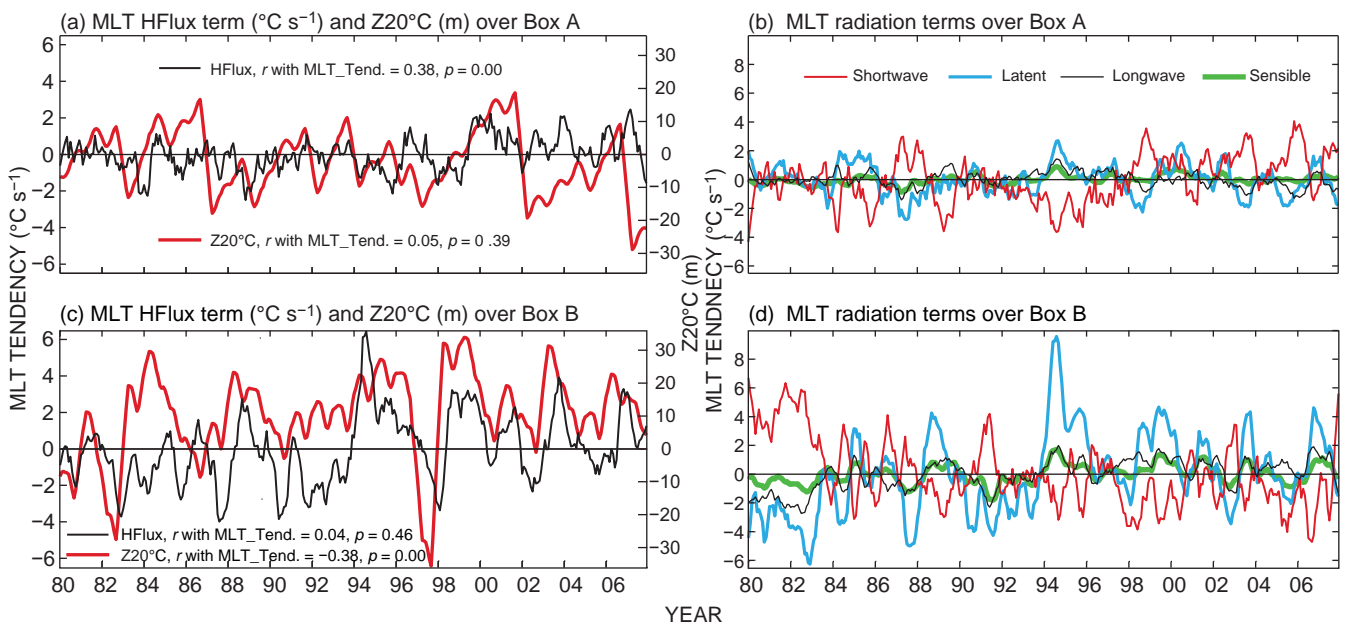


Figure 8: Time-series of anomalies for the mixed-layer temperature (MLT) tendency and thermocline depth over (a, b) the inshore region (Box A) and (c, d) the open ocean (Box B) from the ROMS model (smoothed by a seven-month running mean). Boxes are defined in Figure 5. Positive and negative anomalies indicate elevated and deepened thermocline depth, respectively

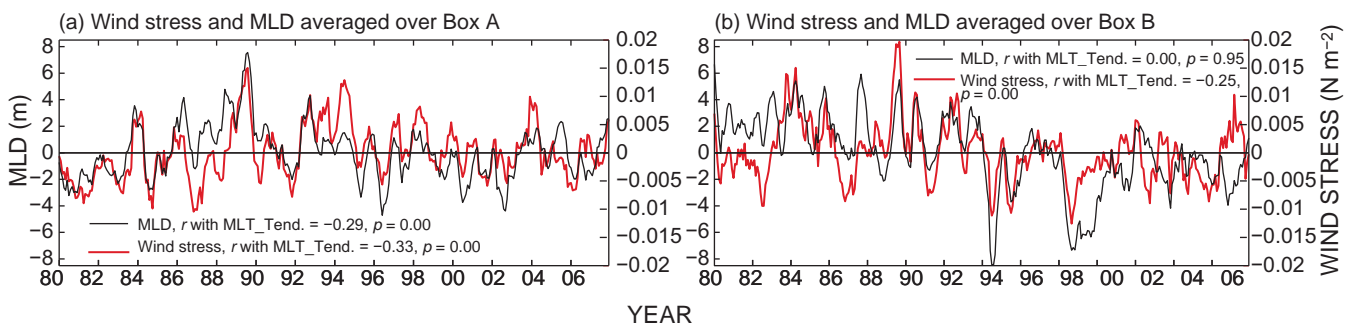


Figure 9: Time-series of anomalies for the mixed-layer depths (MLD) and wind stress over (a) the inshore region (Box A) and (b) the open ocean (Box B) from the ROMS model (smoothed by a seven-month running mean). Boxes are defined in Figure 5

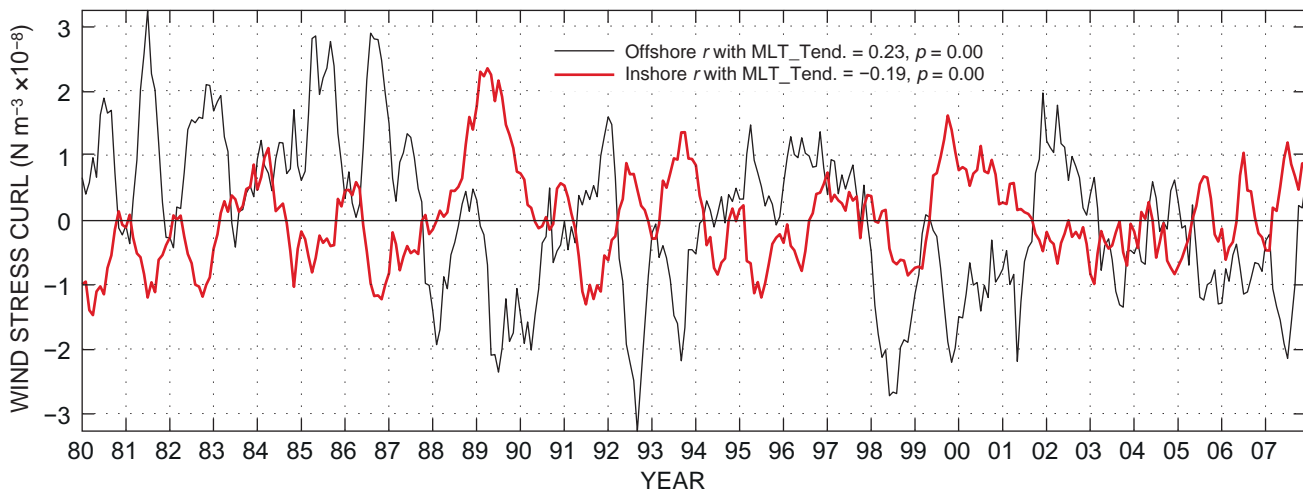


Figure 10: Time-series of anomalies for wind stress curl related to the mixed-layer temperature (MLT) tendency over the Tanzanian shelf region (Box A) and the open ocean (Box B) from the ROMS model (smoothed by a seven-month running mean). Boxes are defined in Figure 5

advected by the mean flow of the NEMC, as implied by Figure 5.

The deepened and elevated thermocline depths respectively occur in strong warm and cool events in the open ocean region (Figure 8c, d). A significant correlation of the interannual variations of the mixed-layer temperature tendency with the thermocline depths occurs in this region. The thermocline depths are deepened during the warm years (1982/1983, 1987/1988, and 1997/1998). The deepest thermocline depth (~35 m) occurs in 1997/1998, the year with the greatest positive SST anomalies in the region. Furthermore, strong negative anomalies of wind stress and mixed layer occur in the offshore region (Figure 9b), which results in the negative wind stress curl (Figure 10) during 1997/1998. Thus, Ekman pumping from local wind stress curl drives partly vertical transport in the offshore region which causes variations of thermocline depths, as suggested by Hermes and Reason (2008, 2009) and Tozuka et al. (2010).

To further investigate the variability of the SST and mechanisms responsible for the SST variability, empirical orthogonal function (EOF) analysis was applied. As shown below, this analysis determines the spatial patterns of the leading modes of the SST in the entire domain, as well as their linkage to the global large-scale modes of climate variability.

The leading SST modes and their linkage to large-scale climate variability modes

An EOF analysis was used for the identification of the leading modes of spatial and temporal interannual variability of SST in the tropical western Indian Ocean. It was performed on the monthly SST anomalies over the study domain for the ROMS model and AVHRR (Figure 11). The first two leading modes that explained about 61% of the total variance were retained.

The first mode explains about 48% of the total variance with a near-homogeneous spatial pattern (Figure 11a). Strong spatial loading patterns occur between 2° N and

6° S, the region with strong SD in the open ocean. The first principal component time-series (PC1) of the SST EOF correlates with the Niño3.4 index and the DMI with r -values of 0.54 and 0.35 ($p < 0.05$ in both cases) respectively. There are similar patterns in the first EOF of the AVHRR SST data explaining about 40% of the total variance (Figure 11b). The difference in the total explained variance could be explained by the differences in spatial and temporal resolutions between the model and AVHRR data. The first spatial pattern mode and its principal component time-series may also be related to the ENSO and the IOD signals. The principal component time-series of the first EOF for ROMS and AVHRR are correlated ($r = -0.73$, $p < 0.05$).

The second mode explains about 13% of the total variance with a north-south oriented dipole spatial pattern (Figure 11c). The same spatial structure is displayed in the second SST EOF of the AVHRR data, and it explains about 8% of the total variance. The first two leading modes of the EOF SST in the AVHRR data collectively explain about 48% of the total variance. The principal component time-series of the second EOF for ROMS and AVHRR are correlated with each other ($r = -0.64$, $p < 0.05$). The second principal component time-series (PC2) in the model is not correlated with either the ENSO or the IOD. It shows a strong warming signal in the Tanzanian shelf region and cooling in the open ocean region in 1987. The former region shows the deepened thermocline as a dominant forcing, as shown in Figure 8c.

Figure 12a, b shows that signals near 64 months (5.3 y) and 32 months (2.7 y) are significant in the model PC1. The 64-month signal can be seen in the AVHRR PC1, but it is mostly outside the cone of influence (Figure 12b). The difference could be associated with the finer temporal and spatial resolution of the AVHRR data compared to the ROMS data. Figure 12c, d indicates that the PC2 presents a dominant signal around the 32-month period for both ROMS and AVHRR. The periods of 5.3 and 2.7 y reflect interannual variability of the ENSO or the IOD, the prominent modes in the tropical Indian Ocean.

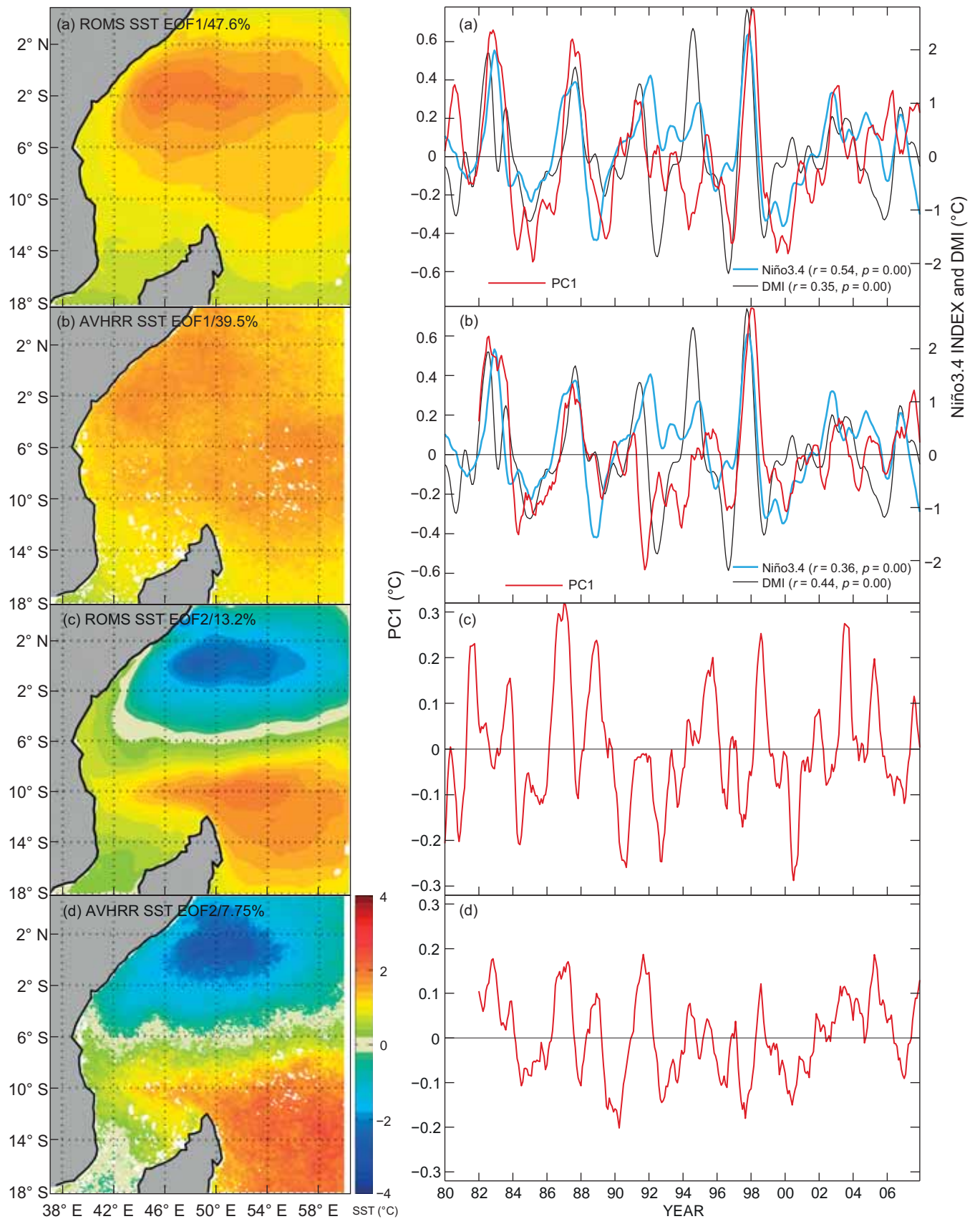


Figure 11: The first two EOF modes for EXP_REF in the tropical western Indian Ocean (left column) and their corresponding principal component time-series (right column; in red). The DMI (in black) and the Niño3.4 index (in blue) are added (smoothed by a seven-month running mean); (a) ROMS EOF1, (b) AVHRR EOF1, (c) ROMS EOF2 and (d) AVHRR EOF2

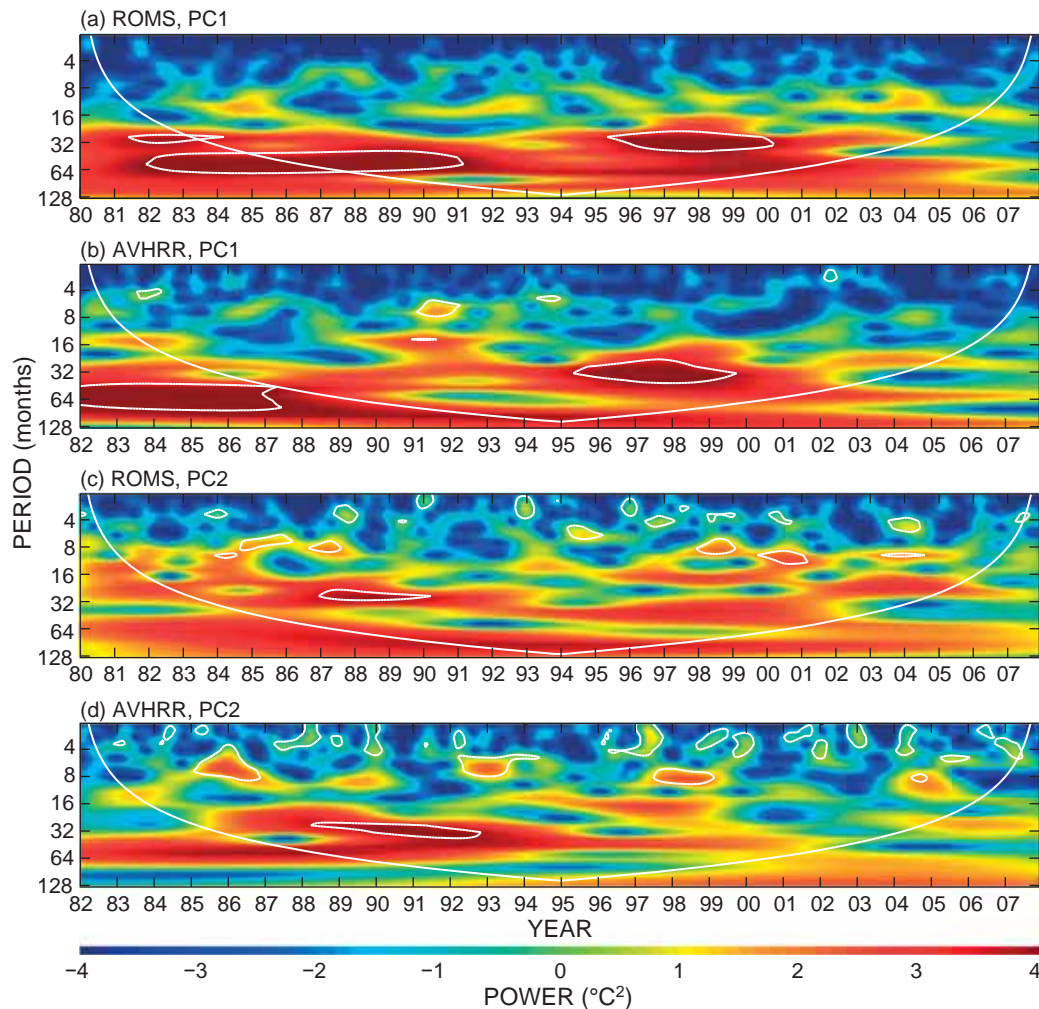


Figure 12: Wavelet power spectrum and power of the wavelet analysis of the first principal component of SST (PC1) from (a) the model and (b) AVHRR and the second principal component of SST (PC2) from (c) the model and (d) AVHRR. The cone of influence and the 95% confidence level contours are indicated by thin white lines

Figure 13a, b suggests that there is strong propagation via Rossby waves of positive anomalies of the SST and SSH from the east, which influence the coastal waters, particularly from 1987 to 1988, 1997 to 1998 and 2002 to 2003. The strongest propagation of the positive SST and SSH occurs in 1997/1998. During the 1997–1998 event, local Ekman pumping partly plays a role in the thermocline anomaly, as suggested by Tozuka et al. (2010), in addition to Rossby waves. Further Rossby wave influences appear through the westward propagation of the positive anomalies of the SST and SSH through the open ocean region in 1982/1983 and 1997/1998 (Figure 13c, d). Thus the 1997/1998 period shows one of the stronger Rossby wave signals and local Ekman pumping during the studied period. These waves are generated by wind anomalies in the eastern Indian Ocean during ENSO and IOD events.

Strong variations of the interannual SST in the tropical western Indian Ocean and their relation with the ENSO and IOD signals can be obtained by stratifying them in calendar months. This is because the influences of the ENSO and IOD in the tropical Indian basin are locked to the seasonal

cycle. Figure 14 displays the monthly correlation of PC1 with the DMI and the Niño3.4 index for the model and AVHRR data. The PC1 in the region mostly correlates with the Niño3.4 index ($r = 0.64$ in the ROMS model and $r = 0.46$ in the AVHRR SST data, $p < 0.05$ in both cases) when the Niño3.4 index lags behind the first SST PC by 3–4 months. The PC1 in the region correlates with the DMI with r -values of 0.41 and 0.45 ($p < 0.05$ in both cases) when the DMI lags behind the PC1 by 2–3 months in the model and by 1–2 months in the AVHRR data respectively. Monthly correlations between the principal component of the first SST EOF and the DMI indicate significant correlation during August to January, peaking in November ($r = 0.61$) (Figure 14a, b). The Niño3.4 index and the PC1 show a significant correlation during the whole year, with high values in October through to January (Figure 14c, d). Thus, strong variations of the interannual SST variations in the tropical western Indian Ocean relate to the local surface forcing as well as to remote forcing induced by the ENSO and the IOD signals.

In summary, the Tanzanian shelf region shows weaker interannual SST variability than the open ocean. This

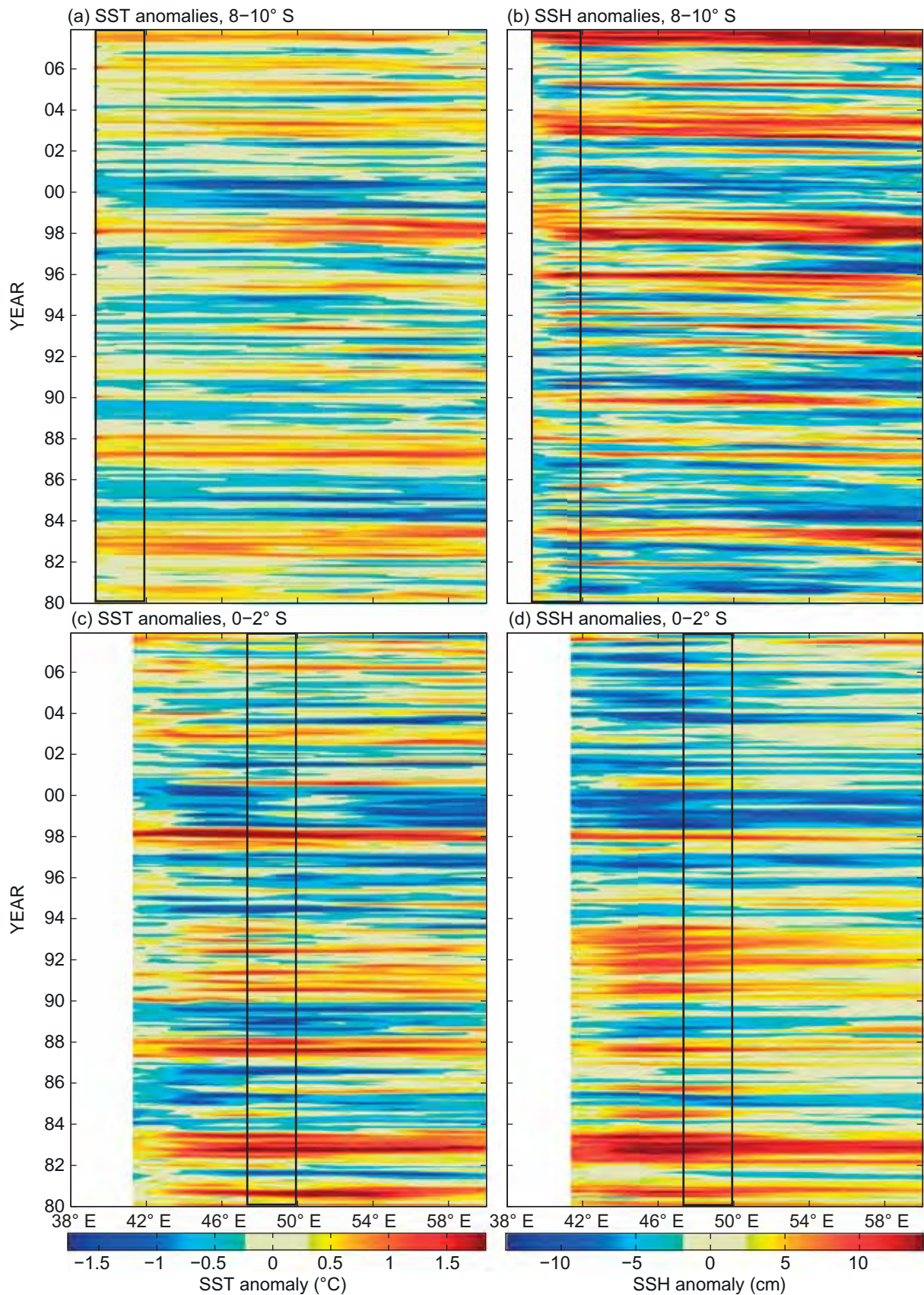


Figure 13: Hovmöller plots for REF_EXP in the tropical western Indian Ocean from the coast at 38° E to 60° E for monthly anomalies, averaged over 8°-10° S, of (a) SST and (b) SSH. The black rectangle shows the coastal location A. Plots (c) and (d) averaged over 0°-2° S of SST and SSH respectively. The black rectangle shows the open ocean location B

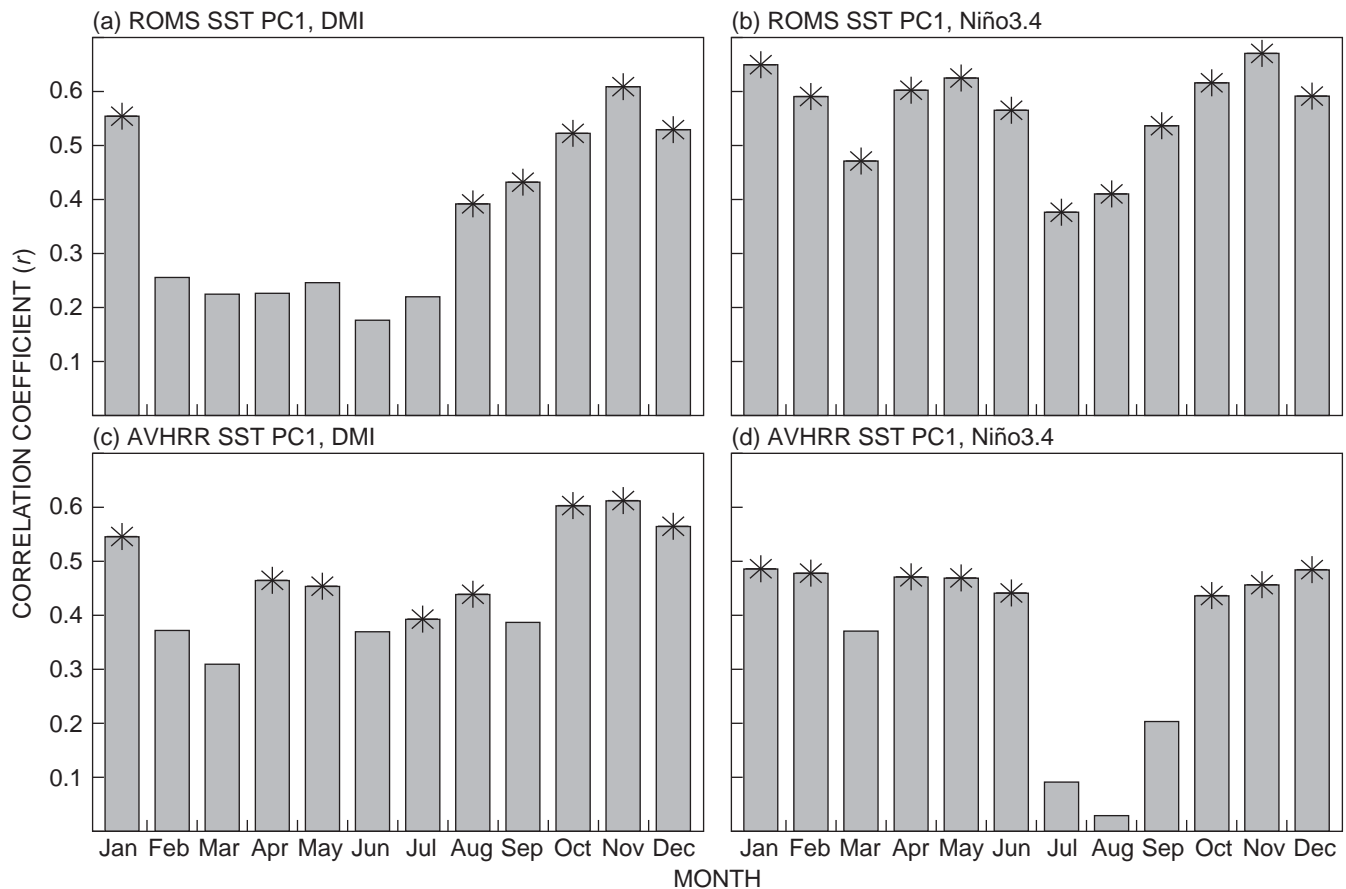


Figure 14: Monthly correlation coefficients between the first principal component (PC1) of the EOF of the SST with the DMI (left column) and the Niño3.4 index (right column) for (a, b) the ROMS model and (c, d) AVHRR. Asterisks indicate significant correlation at the 95% confidence level

suggests different SST forcings in these two regions. Variability in the surface heat fluxes and the thermocline appear to be associated with the interannual SST variability in the Tanzanian shelf region and the open ocean respectively. Thus, it is useful to investigate their relative contributions (see below).

Sensitivity experiments

In order to gain more insight into the relative contributions of the local surface heat fluxes and lateral boundary conditions to the variability in the tropical western Indian Ocean, sensitivity experiments were conducted in the region. The monthly SST anomalies from the control experiment (EXP_REF) were compared with the monthly SST fluctuations from the sensitivity experiments. The surface forcings are kept at climatology in EXP_CLIM_FLUX, whereas the lateral boundary conditions are kept at climatology in EXP_CLIM_SODA.

Figure 15a shows the reduced magnitude of the monthly SST anomalies to less than ± 0.2 °C in EXP_CLIM_FLUX throughout the whole study period (1980–2007), and it is much smaller than in the control and EXP_CLIM_SODA experiments in the Tanzanian shelf region. On the contrary, the monthly SST anomalies from EXP_CLIM_SODA are

very similar to those for EXP_REF, except during the period 1998–2000. A strong reduction of the SST anomalies in EXP_CLIM_FLUX in the shelf waters appears also in the first EOF analysis of the SST anomalies (Figure 16). Values close to zero appear in the Tanzanian shelf region in the first EOF for EXP_CLIM_FLUX. Such patterns suggest a strong relationship between the surface heat fluxes and SST anomalies in the region. The EOF analysis of the monthly SST anomalies for EXP_CLIM_SODA in the Tanzanian shelf waters reflects that of the control experiment with smaller values (< 1 °C) in the spatial patterns (Figure 17). In general, the sensitivity experiments demonstrate that the surface heat fluxes are the dominant forcing of the weaker SST interannual variability in the Tanzanian shelf region.

In the open ocean, the monthly SST anomalies from EXP_CLIM_FLUX and EXP_CLIM_SODA show that the local surface forcing and lateral boundary conditions both exert notable influence (Figure 15b). Given that the mixed-layer temperature tendency shows no significant relation with the surface latent heat fluxes, the influences of the surface forcing can be associated with the local Ekman pumping from wind stress curl. The monthly SST anomalies for EXP_CLIM_FLUX are reduced to about 50% in 1982–1983 and 1987, whereas such anomalies are very similar to that for EXP_REF in 1997–1998. The monthly

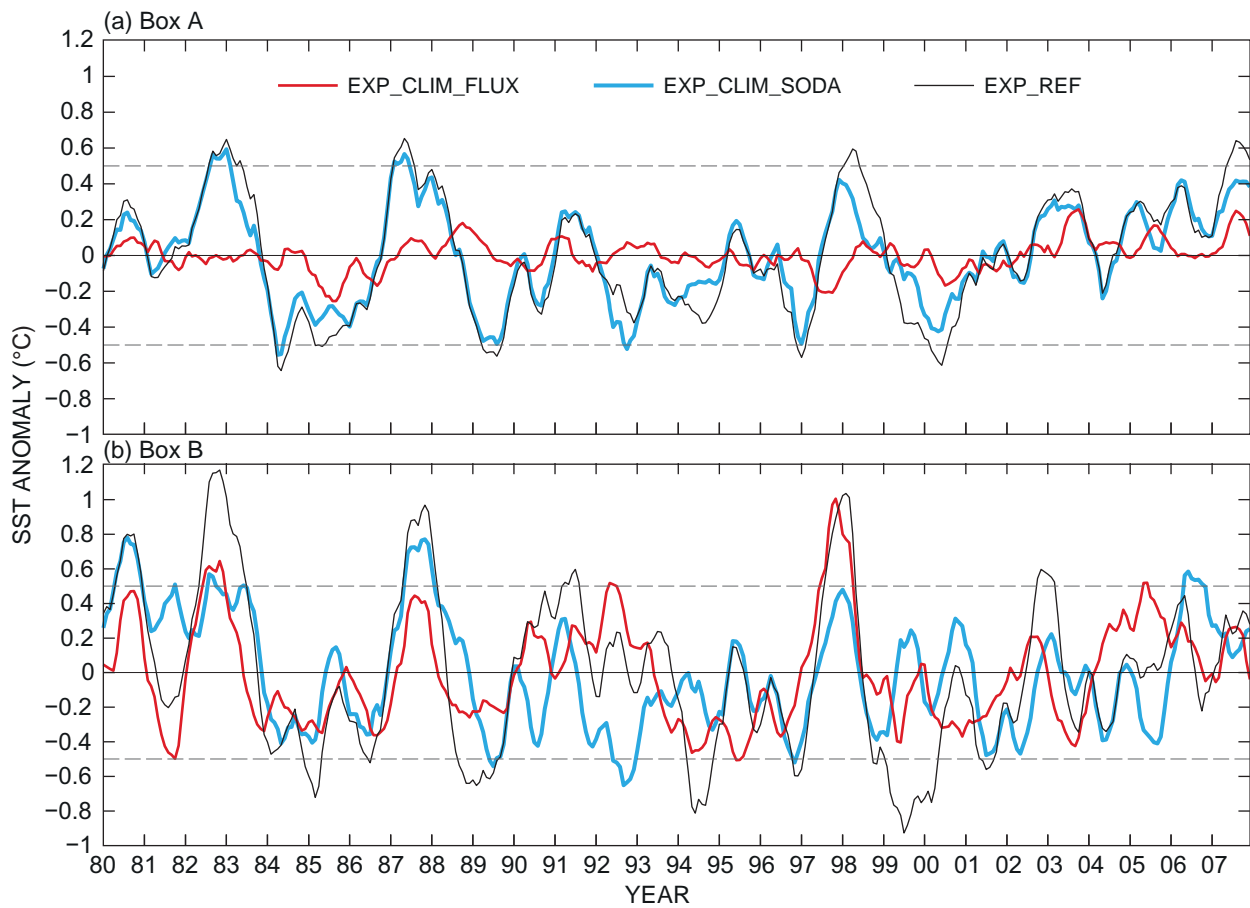


Figure 15: Time-series of SST fluctuations (monthly SST anomalies) from the ROMS model averaged over (a) Box A and (b) Box B for EXP_REF, EXP_CLIM_FLUX and EXP_CLIM_SODA. Boxes are defined in Figure 5

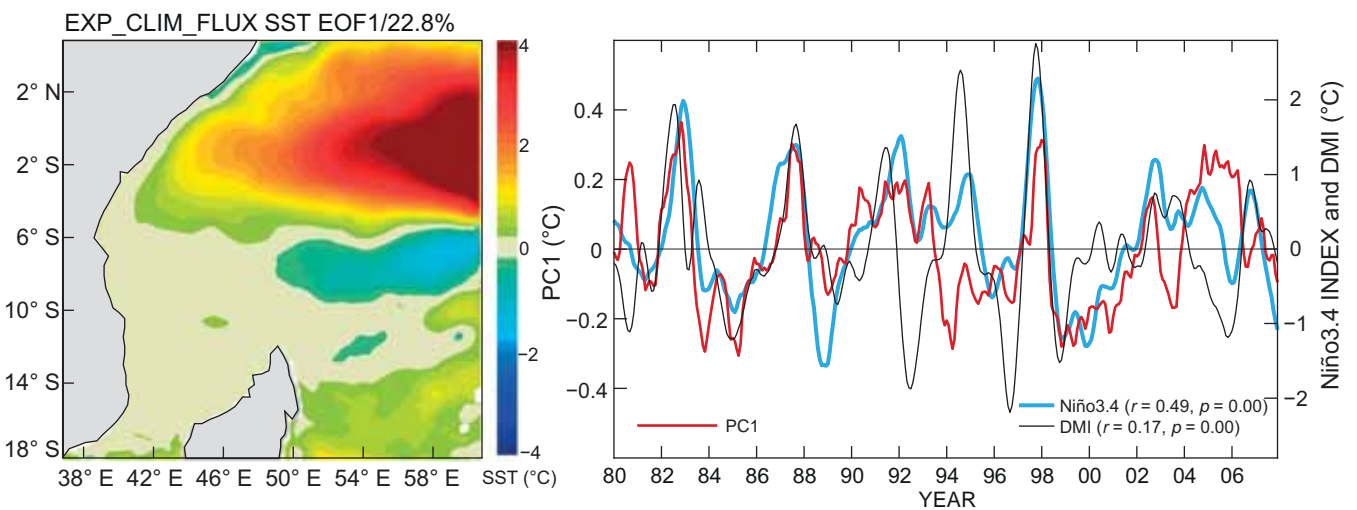


Figure 16: The first EOF mode (EOF1) for EXP_CLIM_FLUX (left) and its corresponding principal component time-series (right). The DMI and the Niño3.4 index are added. The time-series are smoothed by a seven-month running mean

SST anomalies for EXP_CLIM_SODA are also reduced to about 50% in 1982–1983 and 1997–1999, whereas these anomalies are very comparable to that for EXP_REF in 1987. Therefore, these SST anomalies suggest

relatively equal contributions from the local surface forcing and remote forcing. The first EOF analysis of the SST anomalies for EXP_CLIM_FLUX shows increased signals in the open ocean region (Figure 16), showing the influence

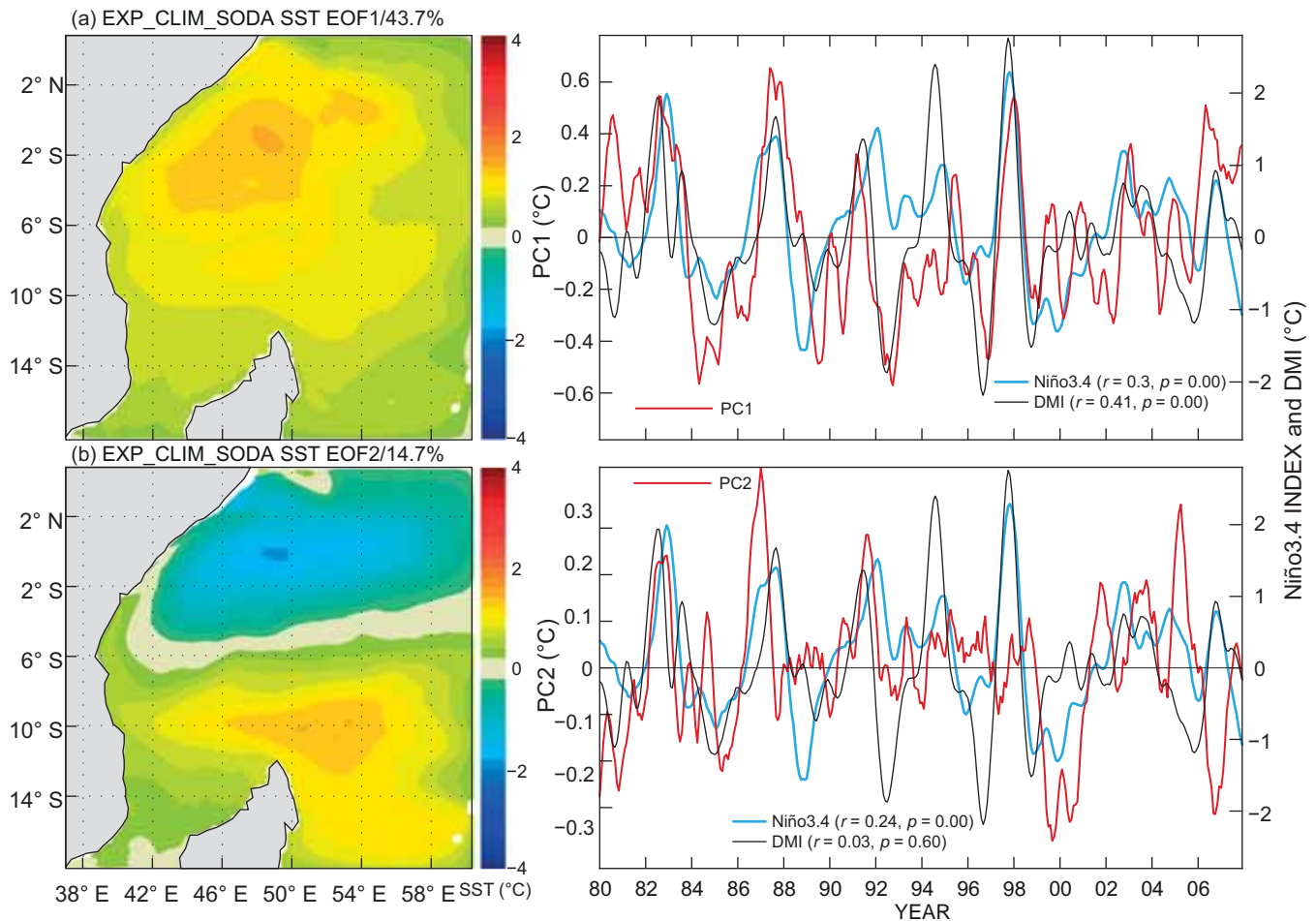


Figure 17: The first two EOF modes (EOF1 and EOF2) for EXP_CLIM_SODA (left column) and their corresponding principal component time-series (right column); (a) ROMS 1st EOF, (b) ROMS 2nd EOF. The DMI and the Niño3.4 index are added. The time-series are smoothed by a seven-month running mean

of the lateral boundary conditions on the variability in the north-east of the model domain. The spatial patterns of the EOF SST anomalies for EXP_REF and EXP_CLIM_SODA are similar, with a smaller amplitude for the first EOF in EXP_CLIM_SODA (Figure 17). This shows that the second mode of variability in the tropical western Indian Ocean in Figure 11 mainly responds to local forcing whereas the dominant mode is influenced by both large-scale and local processes. The first EOF of the monthly SST anomalies for EXP_CLIM_SODA correlates with the Niño3.4 index ($r = 0.3$) and DMI ($r = 0.4$; $p < 0.05$ in both cases). In summary, the sensitivity experiments demonstrate the influence of both local forcing and remote forcing in the open ocean region.

Discussion

The tropical western Indian Ocean experiences strong variability at seasonal and interannual time-scales. Strong, seasonally reversing winds over the region influence the SST in the region. Weak winds occur during transition periods, which correspond with significant SST warming due to reduced evaporative heat loss and mixing. Strong

winds occur in the South-West Monsoon, reflecting significant cooling. During the North-East Monsoon, the north of the tropical western Indian Ocean cools as a result of the dry north-easterly winds from the Asian landmass, whereas there are relatively warm SSTs to the south of the region. However, monsoon winds vary each year and thus impose considerable interannual variability in the region (Webster et al. 1999). Such interannual variability has been associated with ENSO (Reason et al. 2000; Annamalai and Murtugudde 2004; Schott et al. 2009) and the IOD (Behera et al. 2000; Yamagata et al. 2004).

A regional ocean model (ROMS) was used to investigate the interannual SST variations in the Tanzanian shelf region and the open ocean in the tropical western Indian Ocean, for the period 1980–2007. Moreover, the study addressed the interannual SST in the two regions and sought the possible mechanisms responsible for the variability. The model skill in reproducing the variability was reasonably good as the model outputs were in good agreement with satellite data and direct *in situ* measurements. Using sensitivity experiments, the study considered the relative contributions of the surface heat fluxes and lateral boundary conditions to the SST in both regions.

The Tanzanian shelf region experiences weaker interannual variations than the open ocean. The Tanzanian shelf region that extends to the north of Madagascar experiences very small interannual variations of SST, which are significant only at about a 5 y period. However, the strongest interannual variations of SST occur in the open ocean, with two significant periods of about 2.7 and 5 y. These periods reflect the interannual variability of the ENSO and IOD with strong influence in the open ocean. The strongest impacts of the ENSO and IOD signals appear at 2–4 months' lag behind the SST in the region. This is in agreement with Klein et al. (1999) and Reason et al. (2000) who suggested that the tropical Indian Ocean warms one season after a peak in the SST anomalies in the equatorial Pacific. The strongest spatial influence of these large-scale modes appears in the open ocean. Thus, these modes might induce strong influences on the interannual SST through local surface forcing or remote forcing in the region.

In the Tanzanian shelf region, the interannual variability of SST is influenced predominantly by the surface heat fluxes related to shortwave radiation, in conjunction with a contribution from advection by the NEMC. Strong trade winds in the Tanzanian shelf region and to the north of Madagascar carry away the moisture and clouds, leaving the region free of cloud in anomalously warm years. This could be a reason for the positive anomalies in shortwave radiation in 1987/1988 and 1998, and negative anomalies in 1984, 1985, and 1994–1996 that preceded and were out of phase with anomalous latent heat loss. The positive (negative) shortwave radiation anomalies warm (cool) the SST anomalies in the region against the preceding season's cooling and warming, driven by the anomalous latent heat fluxes. The local SST anomalies are then advected by the NEMC mean flow. Hence, weak SST anomalies may result in the Tanzanian shelf region and to the north of Madagascar.

The thermocline depth is closely related to the mixed-layer temperature tendency and SST in the open ocean. Thus, the interannual variations in the thermocline are important for the strong interannual variability of the SST in that region. Periods of deeper and shallower thermocline depths, respectively, occurred during strong warm events in 1982/1983, 1987/1988 and 1997/1998, and during cool events in 1984/1985, 1988/1989, 1996 and 1999/2000. The thermocline variations are induced by local Ekman pumping from local wind stress curl and by remote forcing via Rossby waves associated with large scale variability modes (ENSO and the IOD). The remote forcing is related to ENSO and the IOD in the offshore region because there is a strong correlation between the mixed-layer tendency and SST with the Niño3.4 index and DMI. Thus, anomalous local Ekman downwelling (upwelling) and anomalous downwelling (upwelling) Rossby waves associated with large-scale climate modes (ENSO and the IOD) lead to the deepened (elevated) thermocline, which results in warm and cool SST in the open ocean respectively.

Owing to the marine and coastal contributions to the socio-economic development of Tanzania and its neighbouring countries, understanding interannual SST variability in the tropical western Indian Ocean is important. Such understanding improves planning and management

of climate-sensitive activities in the East African marine ecosystem region and of marine shipping activities in the Tanzanian shelf region.

Acknowledgements — Funding for this research was received from the Carnegie-IAS Regional Initiative in Science and Education (RISE) through the Western Indian Ocean Regional Initiative in Marine Science and Education (WIO-RISE) network.

References

- Alory G, Wijffels S, Meyers G. 2007. Observed temperature trends in the Indian Ocean over 1960–1999 and associated mechanisms. *Geophysical Research Letters* 34: L02606, doi: 10.1029/2006GL028044.
- Behera SK, Krishnan R, Yamagata T. 1999. Unusual ocean-atmosphere conditions in the tropical Indian Ocean during 1994. *Geophysical Research Letters* 26: 3001–3004.
- Behera SK, Salvekar PS, Yamagata T. 2000. Simulation of interannual SST variability in the tropical Indian Ocean. *Journal of Climate* 13: 3487–3499.
- Birol F, Morrow R. 2001. Source of the baroclinic waves in the southeast Indian Ocean. *Journal of Geophysical Research* 106: 9145–9160.
- Carton JA, Giese BS. 2008. A reanalysis of ocean climate using simple ocean data assimilation (SODA). *Monthly Weather Review* 136: 2999–3017.
- Collins C, Reason CJC, Hermes JC. 2012. Scatterometer and reanalysis wind products over the western tropical Indian Ocean. *Journal of Geophysical Research* 117: C03045.
- Debreu L, Marchesiello P, Penven P, Cambon G. 2011. Two-way nesting in split-explicit ocean models: algorithms, implementation and validation. *Ocean Modelling* 49–50: 1–21.
- Ducet N, Le Traon PY, Reverdin G. 2000. Global high-resolution mapping of ocean circulation from TOPEX/Poseidon and ERS-1 and -2. *Journal of Geophysical Research* 105: 19477–19498.
- Fairall CW, Bradley EF, Rogers DP, Edson JB, Young GS. 1996. Bulk parameterization of air-sea fluxes for TOGA COARE. *Journal of Geophysical Research* 101: 3747–3764.
- Han W, McCreary JP, Anderson DLT, Mariano AJ. 1999. On the dynamics of the eastward surface jets in the equatorial Indian Ocean. *Journal of Physical Oceanography* 29: 2191–2209.
- Hermes JC, Reason CJC. 2008. Annual cycle of the South Indian Ocean (Seychelles-Chagos) thermocline ridge in a regional ocean model. *Journal of Geophysical Research* 113: C04035, doi: 10.1029/2007JC004363.
- Hermes JC, Reason CJC. 2009. The sensitivity of the Seychelles-Chagos thermocline ridge to large-scale wind anomalies. *ICES Journal of Marine Science* 66: 1455–1466.
- Jensen TG. 1993. Equatorial variability and resonance in a wind-driven Indian Ocean model. *Journal of Geophysical Research* 98: 22533–22552.
- Kijazi A, Reason CJC. 2009. Analysis of the 2006 floods over northern Tanzania. *International Journal of Climatology* 29: 955–970.
- Klein SA, Soden BJ, Lau NC. 1999. Remote sea surface temperature variations during ENSO: evidence for a tropical atmospheric bridge. *Journal of Climate* 12: 917–932.
- Large WG, McWilliams JC, Doney SC. 1994. Oceanic vertical mixing: a review and a model with a non-local boundary layer parameterization. *Reviews of Geophysics* 32: 363–403.
- Liu Z, Alexander M. 2007. Atmospheric bridge, oceanic tunnel, and global climatic teleconnections. *Reviews of Geophysics* 45: RG2005, doi: 10.1029/2005RG000172.
- Marchesiello P, McWilliams JC, Shchepetkin A. 2001. Open boundary condition for long-term integration of regional oceanic models. *Ocean Model* 3: 1–21.

- Mason SJ. 1995. Sea-surface temperature—South African rainfall associations, 1910–1989. *International Journal of Climatology* 15: 119–135.
- Mayorga-Adame CG. 2007. Ocean circulation of the Zanzibar Channel: a modeling approach. Technical report. La Jolla, California, USA: Theiss Research. Available at <http://www.theissresearch.org/zanzibar/>.
- Meyers GA, McIntosh PC, Pigot L, Pook MJ. 2007. The years of *El Niño*, *La Niña* and interactions with the tropical Indian Ocean. *Journal of Climate* 20: 2872–2880.
- Newell BS. 1957. A preliminary survey of the hydrography of the British East African coastal waters. *Fishery Publications, London* 9: 1–21.
- O'Brien JJ, Hurlburt HE. 1974. An equatorial jet in the Indian Ocean theory. *Science* 184: 1075–1077.
- Obura D, Celliers L, Machano H, Mangubhai S, Mohammed M, Motta H, Muhando C, Muthiga N, Pereira M, Schleyer M. 2002. Status of coral reefs in Eastern Africa: Kenya, Tanzania, Mozambique and South Africa. In: Wilkinson C (ed.), *Status of coral reefs of the world, 2002*. Global Coral Reef Monitoring Network (GCRMN). Townsville: Australian Institute of Marine Science. pp 63–78.
- Ogallo LJ. 1988. Relationships between seasonal rainfall in East Africa and the Southern Oscillation. *Journal of Climatology* 8: 31–43.
- Penven P, Lutjeharms JRE, Florenchie P. 2006. Madagascar: A pacemaker for the Agulhas Current system? *Geophysical Research Letters* 33: L17609, doi: 10.1029/2006GL026854.
- Rao SA, Behera SK, Masumoto Y, Yamagata T. 2002. Interannual variability in the subsurface tropical Indian Ocean. *Deep-Sea Research II* 49: 1549–1572.
- Rao SA, Behera SK. 2005. Subsurface influence on SST in the tropical Indian Ocean: Structure and interannual variability. *Dynamics of Atmospheres and Oceans* 39: 103–135.
- Reason CJC, Allan RJ, Lindesay JA, Ansell T. 2000. ENSO and climatic signals across the Indian Ocean basin in the global context: part 1, interannual composite patterns. *International Journal of Climatology* 20: 1285–1327.
- Reason CJC, Mulenga H. 1999. Relationships between South African rainfall and SST anomalies in the Southwest Indian Ocean. *International Journal of Climatology* 19: 1651–1673.
- Saji NH, Goswami BN, Vinayachandran PN, Yamagata T. 1999. A dipole mode in the tropical Indian Ocean. *Nature* 401: 360–363.
- Schott F, Swallow JC, Fieux M. 1990. The Somali Current at the equator: annual cycle of currents and transports in the upper 1 000 m and connection to neighboring latitudes. *Deep-Sea Research* 37: 1825–1848.
- Schott FA, Xie SP, McCreary JP. 2009. Indian Ocean circulation and climate variability. *Reviews of Geophysics* 47: RG1002, doi: 10.1029/2007RG000245.
- Shchepetkin A, McWilliams J. 2003. A method for computing horizontal pressure-gradient force in an ocean model with a non-aligned vertical coordinate. *Journal of Geophysical Research* 108: 35.1–35.34.
- Shchepetkin A, McWilliams J. 2005. The Regional Oceanic Modelling System (ROMS): a split-explicit, free-surface, topography following coordinate oceanic model. *Ocean Modelling* 9: 347–404.
- Slingo J, Spencer H, Hoskins B, Berrisford P, Black E. 2004. The meteorology of the Western Indian Ocean, and the influence of the East African Highlands. *Philosophical Transactions of the Royal Society* 363: 25–42.
- Smith WHF, Sandwell DT. 1997. Global seafloor topography from satellite altimetry and ship depth soundings. *Science* 277: 1957–1962.
- Swallow JC, Schott F, Fieux M. 1991. Structure and transport of the East African Coastal Current. *Journal of Geophysical Research* 96: 22254–22267.
- Torrence C, Compo GP. 1998. A practical guide to wavelet analysis. *Bulletin of the American Meteorological Society* 79: 61–78.
- Ummenhofer CC, England MH, McIntosh PC, Meyers GA, Pook MJ, Risbey JS, Sen Gupta A, Taschetto AS. 2009. What causes southeast Australia's worst droughts? *Geophysical Research Letters* 36: L04706, doi: 10.1029/2008GL036801.
- Vinayachandran PN, Francis PA, Rao SA. 2009. Indian Ocean Dipole: processes and impacts. In: Mukunda N (ed.), *Current trends in science* (Platinum Jubilee Special Publication). Sadashivanagar, Bangalore: Indian Academy of Sciences. pp 569–589.
- Webster PJ, Moore A, Loschnigg J, Leben R. 1999. Coupled ocean-atmosphere dynamics in the Indian Ocean during 1997–98. *Nature* 401: 356–360.
- Wyrtki K. 1973. An equatorial jet in the Indian Ocean. *Science* 181: 262–264.
- Xie SP, Annamalai H, Schott FA, McCreary JP. 2002. Structure and mechanism of South Indian Ocean climate variability. *Journal of Climate* 15: 864–878.
- Yamagata T, Behera SK, Luo JJ, Masson S, Jury MR, Rao SA. 2004. Coupled ocean-atmosphere variability in the tropical Indian Ocean. In: Wang C, Xie S-P, Carton JA (eds), *Earth's climate: the ocean-atmosphere interaction*. *Geophysical Monograph Series* 147: 189–212.
- Yu W, Xiang B, Liu L, Liu N. 2005. Understanding the origins of interannual thermocline variations in the tropical Indian Ocean. *Geophysical Research Letters* 32: L24706, doi: 10.1029/2005GL024327.